hepia
Haute école du paysage, d'ingénierie et d'architecture de Genève

MSE

Hes·so
Haute Ecole Spécialisée de Suisse occidentale
Fachhochschule Westschweiz
University of Applied Sciences and Arts Western Switzerland

# Optimization of a Hybrid Solar-Geothermal Energy System at Building Scale

A thesis submitted for the degree of

## Master of Science in Engineering

Energy Technologies

By

Romain Sibuet

Under the supervision of
Prof. Dr Nikos Zarkadis

---

Partnership & collaboration with

EPFL

**Laboratory of solar energy and building physics (LESO-PB)**

Prof. Dr Jean-Louis Scartezzini
Dr Roberto Castello
Mrs. Alina Walch

April 2021

**Abstract**

Building sector decarbonisation involves large scale integration of renewable energy sources within the energy mix commonly used to fulfil the heat demand. For this, to combine several energy sources and to control conversion systems based on a systemic approach seems to be promising for making nearly zero energy buildings a standard. Such hybrid energy systems may be more reliable and hence play a key role for grid interaction of variable energy sources. Many case studies have proven this already. However, the most of the analysis have often been made on specific building only. The present work aims to address the impact of hybrid renewable energy system use in a more general way. It prevents experts as decision makers from requiring large input information dataset regarding each individual building, on a given location. This enables to study more easily a whole area in terms of renewable energy potential and deduce energy-related information at urban scale. The district of Aire (GE) in Switzerland is selected as case study. Input datasets are based on national Swiss databases and studies previously performed at national scale. Simplified hydraulic model of space heating system is introduced at single building scale. Coefficient of performance temporal variation is included based on heat supply temperature evolution. Modelling of dynamic system behaviour is performed at monthly-mean-hourly temporal resolution. Energy performances are described throughout self-consumption and self-sufficiency ratio indicators. Furthermore, grid-based electricity use is monitored to compare performance of several system configurations with a reference case, that is without any coupling operation strategy in the frame of a hybrid system. Finally, an optimization procedure is applied for renewable energy based equipment sizing purposes. It appears that beyond a certain storage capacity limit, equipment sizing becomes less attractive in terms of energy performance and maximum surface area available for solar photovoltaic production should be harnessed.

# Acknowledgement

I would like to express my gratitude to the EPFL's supervisors for their availability, support and useful comments. I would like to thank the academic supervisors from HES-SO for their encouragement and assistance on the way. Furthermore, I would like to thank Selin Yilmaz and the Chair for Energy Efficiency at University of Geneva for sharing the hourly electricity demand profiles for the residential and service sectors that were used as part of this work. Overall, I would like to thank the HES-SO school for providing courses and solid abilities for my professional path. Finally, I would like to thank my relatives to have been able to endure some hard situations due to my personal commitments and for their long-term support.

# Contents

# List of Figures

# List of Tables

# 1 Introduction

## 1.1 Motivation and general context

Renewable Energy Sources (RESs) are often related to future and innovation. However, they already existed thousands of years ago. People seem to have used vertical water wheels to produce mechanical work in 200 BC [1]. The use of muscle strength from domesticated animals or the use of their own muscles enabled human beings to cultivate land during a long period of history. Then, to transform crop into food products, water and wind power has been largely employed in the past. All these conversion processes were sustainable. Since wind power, just as well as solar power or some other RES-based power, is intermittent and does not match the energy demand timely, miller's activity was very discontinuous. Therefore, he could work more than sixty hours a week in case of windy weather to offset periods with a lack of wind. The absence of dispatachable power supply system further required flexibility on the demand side. This was understood a long time ago. In a time when governments aim to engage deeply into the energy transition by 2050, it could be useful to look back into the past, to pay more attention to some ancient insights and get inspiration from them for today's challenges.

Fossil fuel-based energy sources have significantly changed the paradigm of energy use. As dispatchable and easy-to-harness energy sources, they allowed a rapid growth of the quality of life at very large scale. Nowadays, they constitute the world's primary energy sources. However, their excessive use harms the environment. The building sector is a huge consumer of fossil fuel-based energy at world scale. Technical efficiency gains only are not sufficient to meet climate change targets. In the residential sector, structural changes have even outpaced efficiency improvement since 2014. These are related to device ownership increasing, greater use of appliances and significant growth in average per-capita residential floor area [2]. This very famous phenomena in conservation and energy economics is named the "rebound effect"[1]. It has long known and is still retrieved today very regularly.

The direct use of fossil fuel-based energy in buildings is mainly due to heating technologies. It is roughly divided between 70 % of natural gas and 30 % of coal and oil. According to its World Energy Outlook, the International Energy Agency (IEA) relies on a phase-out of coal and oil-fired boilers by 2030 and a decrease in natural gas use greater than 50 % by 2050 in its Faster Transition Scenario [3]. To this end, innovative and global approach of building related energy conversion systems is necessary. The use of Heat Pumps (HPs) cuts the yearly energy demand for heating by a factor three or four. However, to replace direct use of fossil fuel-based energy sources by electricity-dependent heating devices could be insufficient. To consider energy efficiency improvement at the whole system scale is more suitable.

Therefore, the combination of cost-effective technologies seems to be relevant to reach the ambitious targets of primary energy saving. This provides a promising approach for RESs integration. Indeed, because of their stochastic nature, RESs need complementary energy sources to form a reliable system. Regarding the utility grid, they cause new issues for system planners. Variable RESs may lead to lack of on-demand generation resources. Moreover, capacity values are complex to compute for Solar Photovoltaic (SPV) or wind power plants. To couple and control two or more RESs and build Hybrid Renewable Energy System (HRES) is currently part of many research works in energy systems (see Sect. 2). Such systems could provide valued aid for managing tomorrow's energy distribution systems.

[1] A full rebound effect specifically because the effect magnitude is close to one. The rebound effect is sometimes named the Jevons paradox, in relation to his work in economy including ecological issue for the first time.

## 1.2 De-carbonising the energy sector

In 2015, The Paris Agreement brought all nations to support a unique cause for the first time. In order to mitigate climate change, the agreement defines a main goal applicable to all, that is to reduce global warming below 2 °C, compared to preindustrial era temperature levels. To reach this goal, 196 countries adopting the agreement had to define a set of measures and submitted their plan in 2020, known as national determined contribution. Since the treaty has been ratified, the emergence of new markets with low or nearly-zero carbon solutions has sparked up into several sectors, such as the building sector.

Nowadays, an enormous $CO_2$ emissions reduction potential remains untapped in the building sector. It is responsible for nearly 40 % of total (direct and indirect) $CO_2$ emissions [4]. Direct emissions are mainly due to heat production. Low or medium temperature heat production equipment often relies on fossil fuel-based energy. Thanks to the enhancements of the building envelope performance, a yearly 2 % decrease of energy demand per square meter is observable since 2010, whereas a more important growth of floor surface is observable over the same period [5]. Subsequently, energy use for heating purposes is growing worldwide. It has reached an all-time high in 2019. In Europe, energy taxation directives could be adjusted to include the power of fossil fuel-based heating systems of less than 20 MW in the close future to break the trend [6].

In the context of RESs, both geothermal, surrounding air and solar sources represent solid alternative methods for heat production. Their use is growing through the world. These primary energy sources can be seen complementary because the two first are dispatchable in contrast to the third one. Geothermal energy is also less variable than ambient air and solar energies. In Europe, use of geothermal energy is expected to grow up to 270 % only over the period 2019-2024 [7]. To be captured and become usable with a temperature range suitable for heat demand, this energy source needs to use mechanical work in most of the cases. This is often done through a HP. Since the latter is electricity-dependant, to include SPV installation into a single HRES appears relevant. This may enable to decrease building $CO_2$ footprint significantly. Furthermore, it is a practical way to limit the electricity demand from the grid, especially when this kind of system is extended at larger scale. For these reasons, such a hybrid system will be studied in the next sections. First, a brief state of the art and market current trends of both two technologies are provided.

### 1.2.1 Geothermal energy and heat pumps

The use of shallow geothermal energy[2] is growing worldwide. An estimation of the annual installed capacity growth[3] is 9.06 % over the period from 2015 to 2019 in 58 countries or regions [8]. In terms of direct use[4] of geothermal energy per land area (installed capacity per 100 $km^2$), Switzerland places itself among the five leaders in the world, together with Iceland, Sweden, Hungary, and Austria [8]. Although Ground Source Heat Pump (GSHP) utilisation has started since the 1980s in Switzerland, it has really increased since the decade of 2000s. In 2017, all vapour compression systems represent about 18 % of the Swiss heat production equipment [9]. The current trend reveals this figure is still increasing, benefiting from removal of fossil fuel-based heat production systems. Mainly due to their performance reliability and versatility, most of them combine Borehole Heat Exchanger (BHE) with HP. Some projects allow to store thermal energy into the ground during periods when heat is in excess or can be considered as waste, thus extending the lifetime of geothermal source. However,

[2] Geothermal energy until 400 m depth.

[3] The annual compound growth rate of installed capacity more accurately.

[4] This means to provide end-use heat from heat into the subsurface. It may be performed through heat pump or without any intermediate equipment for bathing and swimming, greenhouse heating, etc.

GSHPs can imply heavy initial investment whereas they have a low capacity factor[5].

By capturing thermal energy from a natural resource, HPs are indisputably part of the family of devices leading to sustainable buildings. The share of HPs in the heating production technologies worldwide increased since 2010 by representing, added with other renewable heating technologies such as solar thermal collectors, more than 10 % of overall sales in 2019 [7]. This still should be multiplied by more than two until 2030 to be in line with IEA's Sustainable Development Scenario.

As a result, the energy mix for electricity production becomes a critical input regarding whole energy conversion system based on HP application. Therefore, it may become necessary to include electricity generation efficiency to analyse such heating device and judging its real greenhouse gas emission saving effect. To this aim, the European parliament has defined a primary energy-based efficiency ratio for vapour compression systems. A calculation procedure of the share of energy considered to be captured by RES requests to make sure $COP_{seas}$ fulfils the following criteria [10].

$$COP_{seas} > \frac{1.15}{\eta}$$

Seasonal coefficient of performance, $COP_{seas}$, represents the ratio of yearly heat provided to the consumer to the electricity used by the HP. The symbol $\eta$ is defined as the energy conversion ratio between total gross production of electricity and primary energy consumption. When electrical energy is delivered from the national grid in Europe, it is commonly accepted that $\eta = \eta_{grid} = 0.4$. This leads to a criteria such that $COP_{seas} > 2.875$. When HP operation does not comply with the criteria for a given year, energy captured should not be taken into account as part of energy captured from RES.

The energy conversion ratio can be seen as a primary energy conversion factor, $PEF$, such that $PEF = \frac{1}{\eta}$, thus $PEF_{grid} = 2.5$ inside the European Union. Electricity based on SPV plants is considered directly in its secondary form in energy statistics. This yields to $PEF_{PV} = \eta_{PV} = 1.0 < COP_{seas}/1.15$. This artefact lowers the exigence criteria for the calculation of the energy captured from RES for SPV based electricity driven HPs. Therefore, SPV gains leverage as electricity generation system. Therefore, coupling HP with SPV is relevant according to [10].

### 1.2.2 Solar photovoltaic energy and grid curtailments

In these last years, the decrease of installation cost and efficiency improvement caused a world wide spread of SPV panels. Today, it is the second RES for grid-connected electricity generation in the world, behind wind in terms of capacity installed. Since 2000, global SPV installed capacity has grown in accordance with a compound annual growth rate of 43 %. Due to the abundance of the resource and cost competitiveness, it is expected that SPV power installation grows more than six times until 2030 [11]. The technology benefits mostly from national policies and supportive measures, in addition to consumer engagement within the energetic transition.

Grid-connected SPV power supply has however drawbacks. Its non-dispatchable nature and stochastic behaviour are the main part of them. In order to build a supergrid, smartgrid, or microgrid, in association with storage equipment and advanced energy management systems for SPV long term integration into the grid is currently a topic subjected to very active research work. In some cases, the installed capacity growth of SPV plants leads to an increase in frequency and requires active power control for the grid due to power supply fluctuations.

[5] Yearly full load (equivalent) hours divided by 8760. To harness geothermal energy in the aim of providing electricity has a much higher capacity factor for example.

In Europe, the synchronous grid consists of three kinds of reserve power : the operating reserve, frequency-response reserve and replacement reserve. To enlarge replacement reserve in response of RES grid integration demand has been mostly undertaken until today in many countries. Several works focus on demand side action for balancing purposes. One idea is to centrally control electricity-dependent heating systems over large areas. This ancillary service could be included within the non-spinning reserve and procure a great asset for grid reliability improvement. In addition, the electrical storage domain thanks to stationary battery storage system[6] is a complementary approach to reduce grid request. It provides a way to prevent SPV power generation sudden loss in case of objective natural conditions change. Despite the recent lithium-ion battery type apparition, battery storage system capacity remains limited and the additional cost it implies still seems to be an emotional boundary for clients [12].

## 1.3 Swiss regulations

The area selected for this case study is located in Switzerland. The country engaged in tackling global warming several decades ago. Four years ago, Swiss citizens approved the Energy Strategy 2050 [13]. It allows application of the last revision of the Federal Energy Act suggested by the parliament. In this form, the text introduces different mechanisms to adapt existing national framework to the new challenges triggered by climate change. It provides several measures to reinforce domestic RES deployment and integration. With the the Federal Electricity Supply Act's ongoing revision, the goal is to allow opening of the electricity marketplace for all the consumers. The prosumers community group is addressed for the first time in a legal context. It is probably a milestone in terms of energy policy, being the first step of distributed energy system large deployment in Switzerland. This is a promising way to include non-dispatchable RES based generation systems into the grid such SPV installations. The reinforcement of the incentives for consumers to become prosumers is also addressed. In fact, the key proposition is that several prosumers can group together to create a prosumers community. They sign off an agreement. The prosumers community becomes a single consumer for the utility. The community thus receives a unique bill from the utility for the difference between the electrical energy consumed from the grid and the electrical energy provided to. Due to the current buying tariffs, the community hopes to consume its own energy as much as possible, every month. Among the applicable conditions to be considered as a community, electrical domestic production of the community should be at least 10 % of its total electricity demand.

[6] In opposition to non-stationary battery storage system used for motive applications.

# 2 Literature review of hybrid renewable energy systems

An hybrid system is defined as an energy conversion system consisting of two or more energy sources[14]. Distributed HRES can play a significant role to fulfil a large share of energy demand locally, as expected within the framework of many ongoing energy related legal measures. This relies deeply on grid adaptation. The most commonly used RES-based equipments in Switzerland are HP and SPV. They also are well accepted by the population.

The works [15, 16, 17, 14, 18] suggest to combine HP with SPV and Thermal Energy Storage (TES) or Battery Storage System (BSS), and more additional equipments in some cases. The work of Karni Siraganyan et al. [19] considers different types of energy storage technology and analyses the performance with the aid of a specifically developed parametric tool. Key performance indicators cover the economic cost aspect, autonomy level and $CO_2$ emissions. It concludes that SPV installation with BSS does not bring as much autonomy to the system as SPV installation with TES plus HP, and solar thermal integration for providing domestic hot water in addition. To store energy is a way leading to self-consumption increase. TES is recognized as a key element for sustainability and cost-effectiveness aspects. The $CO_2$ mitigation potential obtained from its integration into solar power plant is well known enough [20].

The work of A.T.D.Perera et al. [21] introduces a novel method to optimize HRES including intermittent resources such as SPV and wind energies. It performs multi objective optimization using a combination of energy cost and grid interaction indicator as objective functions.

The article [22] focuses on the optimization of the sizes of hybrid system components like SPV panels, solar thermal collectors and GSHP. It deduces that overall efficiency is highly dependent on the HP capacity and the total area is largely used for SPV generation with a photovoltaic surface larger more than three times the solar thermal surface.

The article [23] investigates on the influence of modelling complexity on key performance indicators for overall energy efficiency. It uses demand response to quantify the electricity flexibility of grid-interactive buildings. The authors need to model both demand side and generation side to simulate a smart micro-grid and then to study energy flexibility. We choose to care about these both sides and to reveal such a flexibility in a more general form.

# 3 Objective and problem framing

The purpose of this work is to study a way to increase both the autonomy and self-sufficiency levels of a building and favour the RES integration. For this, to combine local electrical power supply with electricity-dependent heating system is retained as a promising approach. To this end, an HRES at building scale which includes two technologies SPV and HP is proposed. A daily storage is also added to the system. The hybrid system is compared to the reference system corresponding to the identical equipment without any control algorithm. A specific indicator is defined for this. Finally, an optimisation procedure is applied to the distributed HRES so that the optimal size of both the storage and the domestic electrical power supply is found at single building scale.

Most of the existing studies are specific to a given location. The approach followed here has the ability to be transposable at large scale allowing to study energy sharing management of large area. That's why, the HRES modelled is inspired from widespread technologies in Switzerland. With the aid of this kind of system, such an area could provide an operating reserve enlargement capability, useful for grid regulation. The estimate of such potential could lay the foundations of a future work.

Performance key indicators selected in the present work are self-consumption ratio, $SCR$, self-sufficiency ratio, $SSR$, and grid-based electricity use performance factor, $EPF$. They are defined as follows :

$$SCR = \frac{\sum_t \min\{\dot{E}_{PV}(t),\, \dot{E}_L(t)\}}{\sum_t \dot{E}_{PV}(t)} \tag{1}$$

$$SSR = \frac{\sum_t \min\{\dot{E}_{PV}(t),\, \dot{E}_L(t)\}}{\sum_t \dot{E}_L(t)} \tag{2}$$

$$EPF = \frac{\sum_t \dot{E}_L^{ref}(t) - \min\{\dot{E}_{PV}(t),\, \dot{E}_L^{ref}(t)\}}{\sum_t \dot{E}_L(t) - \min\{\dot{E}_{PV}(t),\, \dot{E}_L(t)\}} \tag{3}$$

Where $E_L$ is the whole electrical energy load, $E_{PV}$, is the Rooftop-mounted Photovoltaic (RPV) based electrical energy supply, and $t$ is the time. The superscript $ref$ relates to the reference case. We have $SCR$ and $SSR$ defined over [0, 1] and $EPF$ is defined over $[0, +\infty[$.

The present work is divided in several parts. First, the data and the case study selected are introduced. The methodology section describes the distributed HRES model and its components. Finally, the results are discussed and perspective for future works are given.

# 4 Data and case study introduction

Inspired from Geographic Information System (GIS) technology, we combine geo-referenced data with survey data to map RES and energy demand of a territory at urban scale. We use the demand services module from the Swiss reference energy system to map hourly demand profile to each building. Then, different energy models are applied to quantify renewable technical potential on the supply side.

## 4.1 Datasets

The final goal is to determine performance on the entire area. For this reason, data is formatted in Monthly Mean Hourly (MMH) resolution. Each time step represents an average value at a given hour of each month, across all days of the month. Thereby we get 288 distinct time steps for a whole year keeping seasonal patterns of the data into account [24]. This enables to limit computational complexity as large datasets need to be combined. This is applied to all data input.

### 4.1.1 Building dataset

General building information is obtained from Swiss National Building and Dwelling Registry (RegBD) maintained by the Federal Statistical Office (FSO). The database contains information about each residential building, identified as a unique entity. The non-residential buildings are not necessarily included in the RegBD. Identifier EGID is assigned to each entity. Then, several mandatory or optional attributes are assigned to each one of them. The registry consists mainly of survey data based on two types of sources. The primary data source results from the collaboration with local authority and the secondary data source is from the collaboration with professional actors. The latter is typically used for registry updates. Table 1 describes the attributes kept for further steps.

| **Attribute identifer** | **Description** |
|---|---|
| GKLAS | Building class |
| GASTW | Number of floors |
| GAREA | Ground surface |
| GKAT | Building category |
| GKODE | Coordinate E of the building |
| GKODN | Coordinate N of the building |

Table 1: Attributes of interest related to each EGID identifier.

### 4.1.2 Heat demand dataset

End-use energy yearly heat demand of each building is obtained from [25]. We use Swiss TIMES Energy system Model (STEM) from [26] to get hourly profiles by sector and typical day which are weekday or weekend in winter season, summer season, or intermediate season. The model is based on various data sources from Switzerland and other countries. For space heating, it borrows typical daily demand curves from Germany and adjusted with Swiss Heating Degree Days (HDD). Hot water demand profiles are based on surveys conducted in Switzerland and Germany [27].

### 4.1.3 Electricity demand dataset

Hourly electricity demand for heating is deduced from COP calculation. Electricity demand for appliances from Joint Activity Scenarios and Modelling (JASM) group [26] is based on [28], and [29] for lightning demand especially. Datasets from 8 countries have been used and specific inputs relative to Swiss context have been

included. Regarding the lightning model, averaged results from 100 homes in UK have been used. All the energy demand patterns consider the least-cost technologies to deliver the required demand from end-use energy. Energy hourly demand is highly dependent on the technology selected to make any energy conversion process and to fulfil service demand in the reality.

### 4.1.4 RPV potential dataset

Technical SPV potential for individual roof surfaces is based on [24]. A methodology which combines machine learning algorithms, GIS and physical models has been developed to obtain technical potential at hourly temporal resolution. Since RPV potential is spatially dependent, the model accounts rooftop geometry, for superstructures, shading effects and sky visibility. The roof surfaces that are shaded more than 60% of the daylight hours are considered as unsuitable surfaces for SPV installation as well as roof with minimum available area lower than 8 $m^2$. The computation uses swissBUILDINGS3D 2.0 as input, a vector based data set created by the Swiss topographical office.

### 4.1.5 BHE potential dataset

Technical geothermal potential from shallow BHEs is based on [30]. The estimation takes into account available area for BHE installation and possible thermal interference when optimal BHE arrangement is not observed. A minimum borehole spacing of 5 m and a maximum borehole depth of 200 m has been applied. Available area is quantified such that all parcels containing at least one building within their boundaries are considered. The surface area is equal to the surface of each parcel from where any built-up areas such that building footprints, roads, railways, parking ..., is removed. Furthermore, a buffer zone of 3 m width from any building footprint edge and parcel boundary is removed to assure a minimum distance from BHE in accordance with SIA [31] recommandations. Regarding Air Source Heat Pump (ASHP), only ambient temperature from Geneva Cointrin station [32] reformatted to MMH is taken as technical parameter.

## 4.2 Data preprocessing

The object DF_UID assigned in the digital model is used for aggregation per building by merging the spatial data to the related roof shape (yellow columns yellow in Table 2). Then, conjunction logical operator is applied to the roof geometries with the whole location geometry so that only the roofs included in the area of case study are retained. Finally, RPV technical potential is summed by EGID (gray column in Table 2), since a building can have several roofs.

| DF_UID | yearly PV potential | ... | yearly PV potential / $m^2$ |
|---|---|---|---|
| 4817431 | 8,928.542 | ... | 769.508 |
| 4817432 | 12,450.400 | ... | 1129.341 |
| ... | ... | ... | ... |

| EGID | DF_UID | GAREA | GKODX | GKODY | ... | geometry |
|---|---|---|---|---|---|---|
| 1004088 | 4817431 | 36.86 | 503503.978 | 134181.171 | ... | POLYGON( ... ) |
| 1004088 | 4817432 | 36.86 | 503500.517 | 134175.889 | ... | POLYGON( ... ) |
| ... | ... | ... | ... | ... | ... | ... |

Table 2: Merging operation representation between the variables of the RPV dataset identified by object DF_UID (on the top) and attribute variables from the roof digital model (on the bottom). Then, grouping operation representation on the EGID identifier column, once the geometry related to the location has been used.

The input dataset from the STEM model, sorted by building category, enables

to create hourly heat demand profiles. This provides hourly coefficients for finding heat load from total yearly heat demand, $Q$. Based on year 2020, a routine code is developed to split the year in 3 seasons and to count the number of weekdays and weekend days for each ones. Basically, winter and summer periods are taken as usual seasons and intermediate season matches to spring and autumn together. The daily heat demand on a typical weekday during the $k$ season is obtained as follows :

$$Q_k^{wk} = Q \sum_{t=0}^{23} \frac{C_k^{wk}(t)}{n_k^{wk}} \tag{4}$$

Where $k$ is one of the three seasons, $n_k^{wk}$ is the number of weekdays during $k$ seasons and $C_k^{wk}$ is the related coefficient from the dataset.

Thus, the average hourly heat demand on a typical day during the $i$ month within the $k$ season is given by the barycentre of $(n_i^{wk},\ (n_k^{wk})^{-1}C_k^{wk})$ and $(n_i^{we},\ (n_k^{we})^{-1}C_k^{we})$. So, we have :

$$Q_{i,k}(t) = \frac{Q}{n_i^{wk} + n_i^{we}} \left( n_i^{wk} \frac{C_k^{wk}(t)}{n_k^{wk}} + n_i^{we} \frac{C_k^{we}(t)}{n_k^{we}} \right) \tag{5}$$

When the $i$ month is divided in two seasons[7] $k$ and $k'$, barycentre $B\Big((n_{i,k}^{wk},\ (n_k^{wk})^{-1}$ $C_k^{wk})$, $(n_{i,k}^{we},\ (n_k^{we})^{-1}C_k^{we})$, $(n_{i,k'}^{wk},\ (n_{k'}^{wk})^{-1}C_{k'}^{wk})$, $(n_{i,k'}^{we},\ (n_k^{we})^{-1}C_{k'}^{we})\Big)$ need to be calculated. The same calculation procedure is applied for each season.

## 4.3 Software and tools

All data are processed by using the open-source code software Python 3.8. Depending on data type, specific data structures are handled for intuitive and concise analysis. We use mostly Pandas and GeoPandas libraries for tabular data returned by spreadsheet or databases. Multi-dimensional arrays are managed thanks to Xarray library and Pyplot API from Matplotlib is used for visualization. Finally, packages such as Numpy or Scipy are used for scientific computing and vectorization.

## 4.4 Geneva case study

Due to data availability and inclusion under the scope of the last regulation, the residential area of Aire, located in Geneva canton, is selected. It is part of the Vernier district as a statistical sub-sector. The sub-sectors have been built by the authorities[8] in the 1990s based on similar statistical observation. After cleaning, dataset allows us to get necessary information about 518 buildings. The area includes mostly Residential Single Family (RSF) buildings, then some Residential Multi Family (RMF) and Service (SER) buildings, in a second place.

Thanks to the previously presented datasets, monthly electricity and heat demand versus monthly renewable energy potential are first compared for the whole area (see Fig. 2). There are 91 out of 518 buildings for which RPV potential is nil and 201/518 buildings for which it is not possible to harness the geothermal energy source. For the remaining buildings, the monthly geothermal demand is computed under the assumption that seasonal coefficient of performance of HP for every building equals 3.0. Although the geothermal potential is very high in comparison to the demand, we need to make sure the borehole location matches the parcel where related building is located. The object UUID assigned to each building footprint or parcel within the topographic landscape model of Switzerland [33] is used to this end. A spatial join operation allows thus to relate each building to its possible geothermal potential.

[7] The march month is divided between winter and spring i.e intermediate season.
[8] GIREC, i.e Interdistrict Groupment for Cartographic Representation.

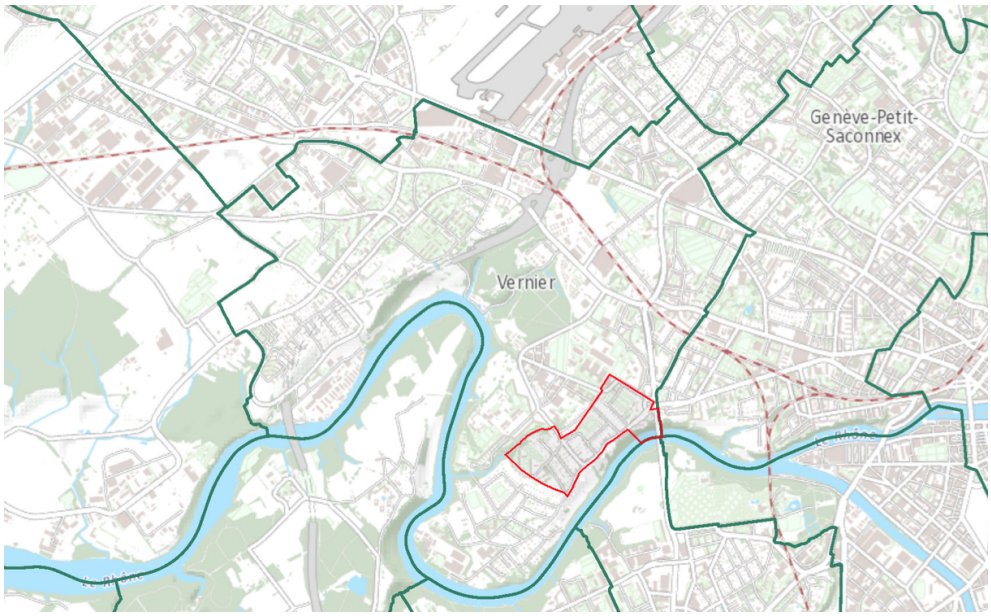


Figure 1: General reference map of Vernier district. The Aire sub-sector is red framed. Scale ratio : 1/25,000.

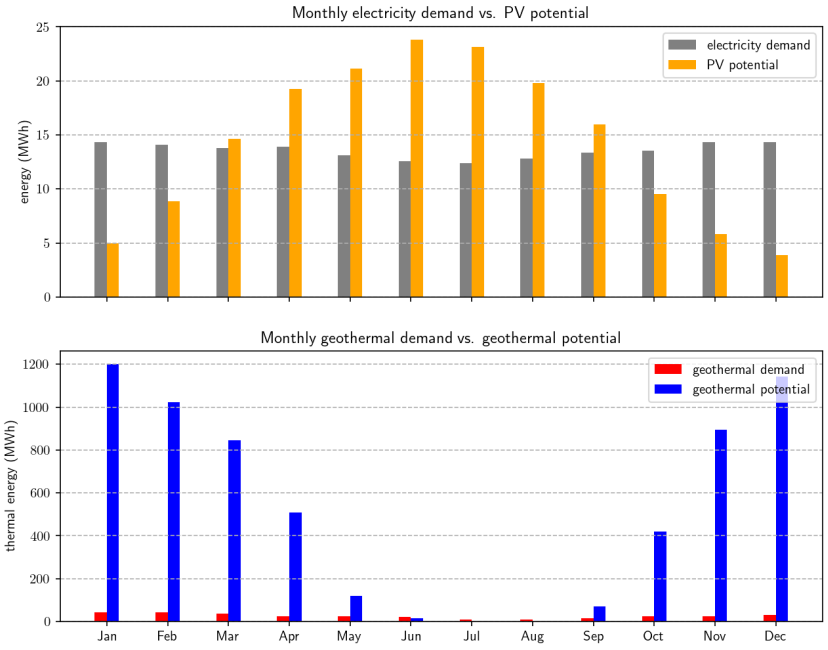


Figure 2: Monthly electricity and heat demand versus monthly related renewable energy potential at urban scale.

# 5 Methodology

In this section, the distributed HRES and its components are presented. First, a bottom-up approach is developed to model energy demand at building scale. Energy conversion system operation is described and general assumptions are mentioned. This methodology can be applied to the 427 buildings with RPV technical potential under previous mentioned assumptions.

## 5.1 System description

The distributed HRES system aims to harness two main energy sources : solar radiation and shallow geothermal heat or ambient air heat, depending on local opportunities. Whatever the heat source, it is extracted through an HP coupled with a RPV installation. Electricity used by the HP is supplied from the solar installation as much as possible. In case of unsatisfactory weather conditions, the electricity grid is used to fulfil the demand. Therefore, electricity final energy demand is divided between electricity based on national energy mix provided by the grid, and electricity based on solar energy provided by RPV installation. The final objective is to increase the solar fraction.

We use TES to bring flexibility and load shift capability to the system. This allows longer heat pump operation during sunny periods even if the current heat load does not match the solar potential. The device is thus able to supply heat demand independently, as long as its energy level is sufficient and its temperature level as high as expected. Finally, the system consists of an additional Electric Heater (EH) in case of geothermal energy lack during peak period.

On Fig. 3, ellipsoid elements indicates energy conversion step and rectangular elements energy source / sink. Gray connection line represents electricity energy flux, blue connection line low temperature[9] thermal energy flux, red connection line medium temperature[10] flux, dark red connection line high temperature[11], and brown connection line other end-use energy form. Blue dashed line (ended by empty circle on a side) means exclusive disjunction between both two related heat sources. It depends on the building selected. Dot line (ended by full circle) means possible conjunction with additional energy conversion equipment, when it is necessary.

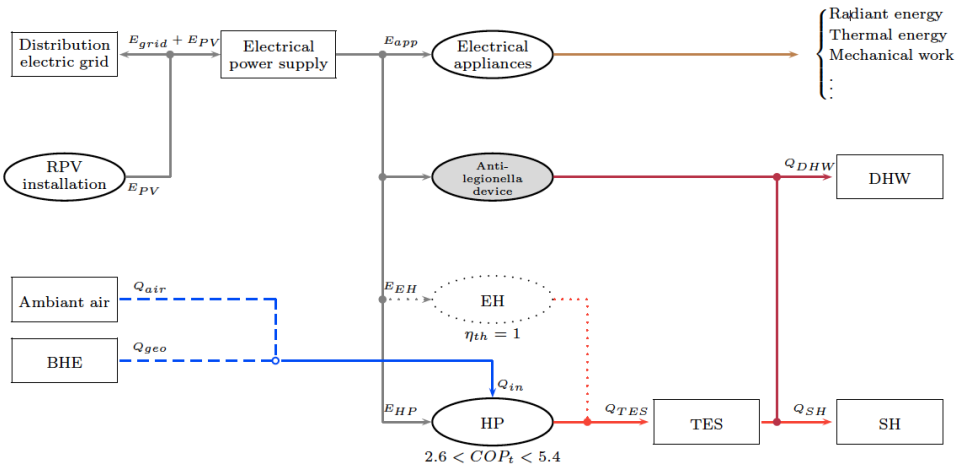


Figure 3: Energy conversion synoptic

[9] Such as $T < 5°C$.
[10] Such as $5 \leqslant T < 45°C$.
[11] Such as $T \geqslant 45°C$.

## 5.2 Hourly heat demand

Since STEM model consists of two day types and three seasons, there are six categories of coefficient. After input dataset rescaling in MMH format[12], annual heat demand is copied by six, that is the number of seasonal coefficients. Element wise multiplication is applied for each demand then, heat load can be directly plotted for each building.

## 5.3 Hydraulic model

Heating supply temperature has a large impact on the heating system performance, especially for HP application. First, heat design load $\Phi(kW)$ is valued through the following equation :

$$\Phi = 0.75 \frac{\max\{Q_{SH},\, Q_{DHW}\}}{2300} \tag{6}$$

Where $Q_{SH}$, $Q_{DHW}$ are the end-use yearly heat demand for space heating and for domestic hot water expressed in kWh, respectively. The heating system is supposed to provide heat either for space heating or for hot water preparation, that's why the maximum value is selected. The denominator is the equivalent number of system full-load running hours per year and is assessed thanks to SIA [34]. The constant factor of 0.75 is applied to the result as it is well known that optimal design load of HP is included in a range of $0.7 - 0.8$ times the full-load due to economic consideration.

It is assumed every heating system uses radiator as terminal device. This is less favourable than floor heating system in terms of temperature supply and system performance. Since we don't know real-time operation of the heating system, we attempt to assess hourly temperature for each subsystem taken separately, i.e for space heating on one side and for domestic hot water on the other. We know the minimum requirement for domestic hot water preparation. Supply temperature to heat domestic water is supposed to be constant. Heating control strategy is supposed to be temperature dependent at a constant flow rate. This is mostly the case for system designed with static heat emitting component. Flow rate can be assessed from design condition with the heat design load previously computed and temperature difference of 10 °C.

A radiator is a heat exchanger between carrying fluid and surrounding air inside a given room. The following expression has been developed by manufacturers specifically for radiator thermal power, $\dot{Q}_{rad}$, evaluation [35] :

$$\dot{Q} = K_{rad} \Delta T_{ln}^{n} \tag{7}$$

Where $K_{rad}(W/^{\circ}C^{n})$ is the radiator constant, $\Delta T_{ln}$ is the logarithmic mean temperature difference, and $n(-)$ is the emitting mode exponent or Rietschell coefficient. The figure enables to include better the combination of radiative heat transfer with convection than by using usual formula $\dot{Q} = UA\Delta T_{ln}$. Based on SIA [34], we take $n = 1.3$.

From (7) and heat thermal power expression (at constant pressure) $\dot{Q} = \dot{m}c_p(T_{sup} - T_{ret})$ for a given time step, we get :

$$T_{ret} = T_{room} + \frac{\frac{\dot{Q}}{\dot{m}c_p}}{\exp\left(K_{rad}^{1/n} \dot{Q}^{1-1/n} \frac{1}{\dot{m}c_p}\right) - 1} = f_n(\dot{Q}) \tag{8}$$

Calculation details are provided in Appendix A. The flow rate and $K_{rad} = UA$ values are taken from the nominal operating conditions. We suppose $\Delta T_{nom} = 30$°C. The result for a typical RSF building located in the study area is given in Fig. 4.

[12] For example, a day MMH in December month is based on 20 days during intermediate season and 11 days during winter season. For the first period, it counts 15 weekdays and 5 weekend days, then for the second period it counts 7 weekdays and 4 weekend days.

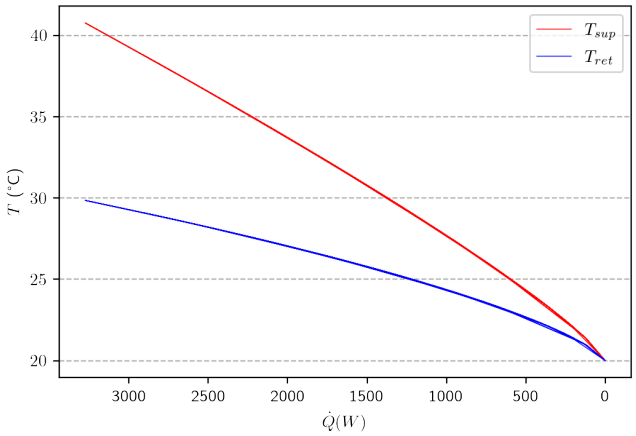


Figure 4: Typical supply and return temperatures heat load dependence of a building located in the study area.

We can note supply temperature is greater when heat load is high than when heat load is low. Moreover, the more the heat load is high, the more the temperature gap between supply and return fluid is large.

## 5.4 Heat production

The heat production system is either GSHP or ASHP, depending on geothermal potential of the corresponding parcel. Every yearly geothermal potential lower than the yearly heat demand supposed (from heat source related to GSHP) involves ASHP selection by GSHP selection replacement. In case of the yearly geothermal potential such condition is found satisfactory, GSHP is selected as main heat production system and a second test condition is performed on peak-demand period, that is on December, January, and February months. Monthy geothermal potential is computed for each building through HDD ratio. Then, daily potential is assessed by number of days per month divison. When daily potential becomes nil before the end of the day, a back-up EH system is implemented in addition to GSHP. Its efficiency factor is taken such that $\eta_{EH} = 1$. This occurs for 9 buildings in the study case.

Heat load variation for the HP involves global electricity load variation. COP variation due to heat source and sink temperature variation is based on [36]. Quadratic regression is performed on manufacturer data under different temperature conditions and for different HP types. Only on-off modulating HPs have been considered in the study. BHE source temperature is considered yearly constant and set to $5°C$. Sink temperature is time dependent and returned by calculation done before (see 5.3). To prevent HPs performance drop, the heat sink temperature necessary to fulfil domestic hot water demand is set to $45^{\circ}C$. Additional anti-legionela electrical device is supposed to daily operate directly into the water tank and is not considered here. Lastly, we consider a temperature difference of $6°C$ for intermediate exchangers as evaporator and condenser.

To perform first and second test condition, thermal energy demand for geothermal source is computed on a monthly or daily basis thanks to the following equation :

$$Q_{geo} = \sum_{t=0}^{t\in\{y,\,d\}} Q_{SH}(t)\left(1 - \frac{1}{COP_{SH}(t)}\right) + Q_{DHW}(t)\left(1 - \frac{1}{COP_{DHW}(t)}\right) \quad (9)$$

Where $Q_{geo}$ is energy from geothermal heat source, $Q_{SH}$ and $Q_{DHW}$, are thermal energy dedicated to space heating and domestic hot water respectively.

## 5.5 Thermal energy storage

TES technical specifications are based on [37]. A cylindrical-shaped water tank with a diameter of 65 cm when storage volume is less than 600 L, or a diameter of 79 cm else is considered. The height is adjusted to match with the tank volume counted for each calculation. Insulated surrounding jacket limits thermal transmittance to $U = 0.41 W m^{-2} K^{-1}$. The following expression is used to compute the thermal losses :

$$Q_{loss}(t) = b\ U\ A(T_{ext}(t) - T_{TES}(t)) \tag{10a}$$

$$A = \pi D \left( h + \frac{D}{2} \right) \tag{10b}$$

Where $D$ is the $TES$ diameter, $T_{ext}$ is the exterior temperature, and $T_{TES}$ is the average TES temperature. The coefficient $b$ is a reduction factor based on [38] due to the storage location supposed to be inside a non-heated room. We have $b = 0.8$.

The maximum temperature of the TES is set to $70°C$, although the COP is low for this temperature level. Charging operation involves electrical power is fed to the HP from the RPV installation only.

The TES is supposed to be daily and ideally stratified that is inner volume can be divided in several distinct layers at fixed temperature rising from the bottom to the top. The storage average temperature is obtained from the following differential equation :

$$\frac{d}{dt} T_{TES}(t) = \frac{\delta Q_{TES}(t)}{C_p dt} \tag{11}$$

Where $C_p$ is the thermal capacity of the fluid and supposed to be constant and equals to $4.185\,\mathrm{MJK}^{-1}$, $Q_{TES}$ is the thermal energy exchanged with the tank.

For a given time step $\Delta t = t - t_0$, this yields to :

$$T_{TES}(t) = \frac{1}{C_p}(Q_{TES}(t) - Q_{TES}(t_0)) + T_{TES}(t_0) \tag{12}$$

## 5.6 System control algorithm

A deterministic algorithm is developed to control TES charging and discharging operation. The strategy is to charge the storage to its maximum with the HP when net RPV production, $E_{PV^+} = EPV - E_L$, is positive. TES discharging operation is triggered as soon as $E_{PV^+}$ is lower than electricity demand, $E_{HP}$, and its average temperature $T_{TES}$ is greater than heat supply temperature for either space heating system or domestic hot water. For a given time step $\Delta t = t - t_0$, TES charging level is computed as follows :

$$Q_{TES}(t) = Q_{TES}(t_0) + Q_{HP}(t) + Q_{SH}(t) + Q_{DHW}(t) + Q_{loss}(t) \tag{13}$$

Electricity demand from HP is based on sink temperature for every time step. Source temperature is supposed to be yearly constant for GSHP whereas exterior temperature is counted for ASHP selection case. Detailed procedure is given in Appendix B. This is applied for each time step $t \in [\![0,\ 287]\!] = \mathcal{T}$. Initial state is set to $T_{TES}(t_0 = 0) = 10°C$ and $Q_{TES}(t_0 = 0) = 0$.

Depending on the storage size and daily RPV-based heat load, several days may be necessary so that the TES charging process reaches an equilibrium. The control algorithm is thus repeated several times for each month until quasi-permanent state condition appears. A specific variable $n$ is defined to account the number of days necessary prior to reach such state condition. The value is mentioned on corresponding charts directly in the next section. The RPV production is supposed to be identical

for every day repeated.

## 5.7 Optimization

Low computation resource optimization method is applied for each building. First, we define decision variable space from the Cartesian product of the two domains $A_{PV}$ and $V_{TES}$, corresponding to RPV surface area and TES capacity respectively. Each one is closed range and its maximum matches to RPV available surface of given building for the first, and storage capacity of 4 000 L for the second. Variation step on each domain is 5 % of the available surface and 200 L capacity. So, the two decision variables $x_1 \in A_{PV}$, $x_2 \in V_{TES}$ browse their respective discrete domains as follows :
$\forall (x_1,\, x_2) \in A_{PV} \times V_{TES}$, $\exists (n_1,\, n_2) \in (\mathbb{N}^2 \cap [0,\, 20]^2) \setminus (\{0\} \times [0,\, 20])$,

$$x_1 = 0.05 n_1 \tag{14a}$$

$$x_2 = 200 n_2 \tag{14b}$$

Since $SCR$ is not defined for $x_1 = 0$, we have $A_{PV} \subset ]0,\, 20]$. Thereby, energy performance can be visualized through three numerical sequences s.a :
$\forall X \in \{SCR,\, SSR,\, EPF\}$,

$$X = (u^X_{(n_1,\, n_2)})_{\substack{n_1,\, n_2 \in \mathbb{N}, \\ n_1,\, n_2 \leqslant 20, \\ n_1 > 0}} \tag{15}$$

These make three equality constrains for each building, which drives easy solving. Finally, affine transformation is applied to each key indicator and linear combination is performed to define $f$ objective function. Output value $y = f(x_1,\, x_2)$ is defined as the variable browsing objective space as follows :
$\forall (x_1,\, x_2) \in A_{PV} \times V_{TES}$,

$$y = a\,(SCR(x_1,\, x_2) - SCR_0) + b\,(SSR(x_1,\, x_2) - SSR_0) + c\,(EPF(x_1,\, x_2) - EPF_0) \tag{16}$$

The $a$, $b$, $c$ and $SCR_0$, $SSR_0$, $EPF_0$ coefficients are used to obtain normalization of the related indicators according to [0, 1]. For each building, these coefficient are defined as follows :

$$a = \frac{1}{\max\{SCR \,|\, (x_1,\, x_2) \in A_{PV} \times V_{TES}\} - SCR_0} \tag{17a}$$

$$b = \frac{1}{\max\{SSR \,|\, (x_1,\, x_2) \in A_{PV} \times V_{TES}\} - SSR_0} \tag{17b}$$

$$c = \frac{1}{\max\{EPF \,|\, (x_1,\, x_2) \in A_{PV} \times V_{TES}\} - EPF_0} \tag{17c}$$

$$SCR_0 = \min\{SCR \,|\, (x_1,\, x_2) \in A_{PV} \times V_{TES}\} \tag{17d}$$

$$SSR_0 = \min\{SSR \,|\, (x_1,\, x_2) \in A_{PV} \times V_{TES}\} \tag{17e}$$

$$EPF_0 = \min\{EPF \,|\, (x_1,\, x_2) \in A_{PV} \times V_{TES}\} \tag{17f}$$

Formulation problem for a given building can be summed up as follows :

$$
\begin{cases}
\text{To maximize :} \\
\qquad f : [A_{PV}^{min},\, A_{PV}^{max}] \times [0,\, 4000] \to [0,\, 3] \\
\qquad\qquad (x_1,\, x_2) \mapsto y \\
\\
\text{Under the constrains :} \\
\quad \exists (n_1,\, n_2) \in \mathbb{N}^2,\, n_1, n_2 \leq 20, n_1 > 0, \qquad (\star) \\
\qquad\qquad x_1 = 0.05 n_1 \\
\qquad\qquad x_2 = 200 n_2 \\
\qquad\qquad SCR = (u^{SCR}_{(n_1,\, n_2)})_{\substack{n_1,\, n_2 \in \mathbb{N}, \\ n_1,\, n_2 \leqslant 20}} \\
\qquad\qquad SSR = (u^{SSR}_{(n_1,\, n_2)})_{\substack{n_1,\, n_2 \in \mathbb{N}, \\ n_1,\, n_2 \leqslant 20}} \\
\qquad\qquad EPF = (u^{EPF}_{(n_1,\, n_2)})_{\substack{n_1,\, n_2 \in \mathbb{N}, \\ n_1,\, n_2 \leqslant 20}}
\end{cases}
$$

# 6 Results and discussion

Calculation procedure previously presented can be applied to 427 buildings located in Aire area. For the results, five buildings are selected and presented hereafter. Among these ones, the last building needs EH during peak-period to fulfil the heat demand. General features of these five buildings are first introduced in Table 3. Line data charts are plotted to exhibit hourly energy demand and production at building scale. Then, behaviour of TES specific charging level, hourly electricity demand and production with use of TES are shown. RPV installation surface is set to 60 % of the maximum surface and TES volume is set to 400 L for each building as a first visualization.

## 6.1 System operation visualization

| EGID | 1029179 | 1028823 | 1029027 | 1028854 | 1029232 |
|---|---|---|---|---|---|
| Sector | RSF | RSF | SER | RMF | RSF |
| Number of floors | 2 | 1 | 3 | 2 | 2 |
| Gross floor area ($m^2$) | 180 | 97 | 618 | 304 | 186 |
| Annual DHW demand ($kWh$) | 1 920 | 2 016 | 5 530 | 3 360 | 5 400 |
| Annual SH demand ($kWh$) | 8 389 | 8 577 | 44 691 | 14 568 | 23 118 |
| $\Phi$ ($kW$) | 3 | 3 | 15 | 5 | 8 |
| Annual electricity demand ($kWh$) | 3 698.6 | 3 698.6 | 11 267.5 | 3 698.6 | 3 698.6 |
| Annual geothermal potential ($kWh$) | 6 104.3 | 30 350.1 | 19 943.8 | 31 841.1 | 19 133.8 |
| Number of roofs | 1 | 2 | 4 | 2 | 2 |
| Roof surface ($m^2$) | 134.1 | 144.4 | 465.8 | 184.6 | 310.5 |
| Annual radiation ($kWh\ m^{-2}$) | 1 301.1 | 2 237.5 | 4 590.7 | 2 008.1 | 2 055.5 |
| SPV suitable roof surface ($m^2$) | 66.5 | 84.5 | 199.4 | 91.5 | 184.4 |
| Annual SPV technical potential ($kWh$) | 6 945.2 | 12 390.4 | 23 490.7 | 11 478.7 | 24 757.9 |
| Heating equipment | ASHP | GSHP | ASHP | GSHP | GSHP |

Table 3: Main features of selected buildings for data visualization.

On the Fig. 5 to 9, each tick locator on the horizontal axis matches midday on a typical day for each month. On the vertical axis, several modelled measures are plotted. For RSF and RMF buildings, in Fig. 5, 6, 8, and 9, the hourly heat demand charts show mainly two peaks per day (for each month) for each demand type. The first one is located at early morning followed by a daytime demand roughly maintained to a high level. The second one appears during the evening and is lower than the first one. The maximum values match with the seasonal pattern. Heat demand for domestic hot water preparation is less seasonal-dependent but more variable during daytime due to household activities (cooking...). During night-time, heat load is almost nil. The two peak demands can be attributed to showers and baths taken the morning and the evening, respectively. In Fig. 7, the hourly heat demand profile is different due to the building category difference. For space heating, the profile shows a single main peak per day related to heating system restart every morning. The heat demand for domestic hot water is overall much lower than heat demand for space heating.

On the second chart in every figure, we can observe hourly electricity demand and RPV hourly potential. The latter is nil during night time. Daily peak production is located between 11 : 00 and 13 : 00, depending on the season. Yearly peak production

is located during summer season. Electricity demand for commonly used appliances is plotted in gray dashed line. The plain line in same color shows additional demand due to the use of electricity-dependent heating device (either ASHP, or GSHP, or EH). Despite the both heat demands in Fig. 5 and 6 are very similar, the global (plain line) electricity demand profiles are different. Indeed, we can note the additional electricity demand caused by the ASHP operation in the first building is higher than in the second one. This is due to a lower $COP$, during winter and intermediate seasons especially. For SER building (in Fig. 7), RPV potential is lower than electricity demand all over the year with selected installation surface. Electricity demand and RPV potential hourly profiles chart within Fig. 9 shows EH back-up operation during January and February months. This is triggered to prevent geothermal source from over-exploitation during heating peak period. Magnitude signal reduction of EH operation is observable thanks to TES use in the fourth related chart. Intermittent operation is also observable when heat demand is high enough during intermediate season and TES has been charged up during several consecutive days (i.e $n > 0$).

Both two last charts of each figure exhibit behaviour change of the system due to control algorithm implementation. On the third chart in every figure, TES charging level signal under quasi-permanent condition only is shown. The number of days necessary to reach such condition is mentioned through the $n$ variable. Charging level at the beginning of each day is thus positive the most of the time, and discharging process can be sometimes observable during the first part of the day. This because the tank charging level is not empty at the beginning of the day and has been charged the day before. Vertical lines are plotted to separate each day and make easier the reading of the chart. During winter season, restriction on TES charging operation is observable in all the cases due to RPV potential limitation, although tank capacity considered here is low enough. During summer season, TES charging operation is completed in all the cases except in Fig. 7.

The use of energy storage leads to the increase of electricity demand for each time step when the excess electrical power is positive in corresponding reference case. Thereby, the TES is charged up to a daily maximum value, according to its capacity and the maximum possible heat production based on either the current SPV electrical power supply or the maximum heat load for the HP. Then, it is priority discharged when electricity production decreases in the aim of saving the energy. TES discharging operation suddenly stops when average temperature is lower than heat supply temperature. A slight descending slope is sometimes notable on storage charging level signal due to thermal losses. On TES charging level chart within Fig. 7, auto scaling drives a vertical axis scale very different compared to the scale of same charts related to other buildings. Basically, charging level signal variation from spring to autumn is due to exterior temperature evolution ; charging operation from ASHP never occurs in the present configuration. The $COP$ variation due to source (when heating equipment is ASHP) and sink temperature variation may drive change on power demand signal. The slope moves sometimes independently from RPV production signal pattern. This is particularly visible on fourth chart within Fig. 9.

Overall, electricity demand hourly profile including HP operation relies more on RPV production after control algorithm implementation. This for charging storage tank purpose. Then, grid-based electricity use can be reduced with the aid of TES discharging operation.

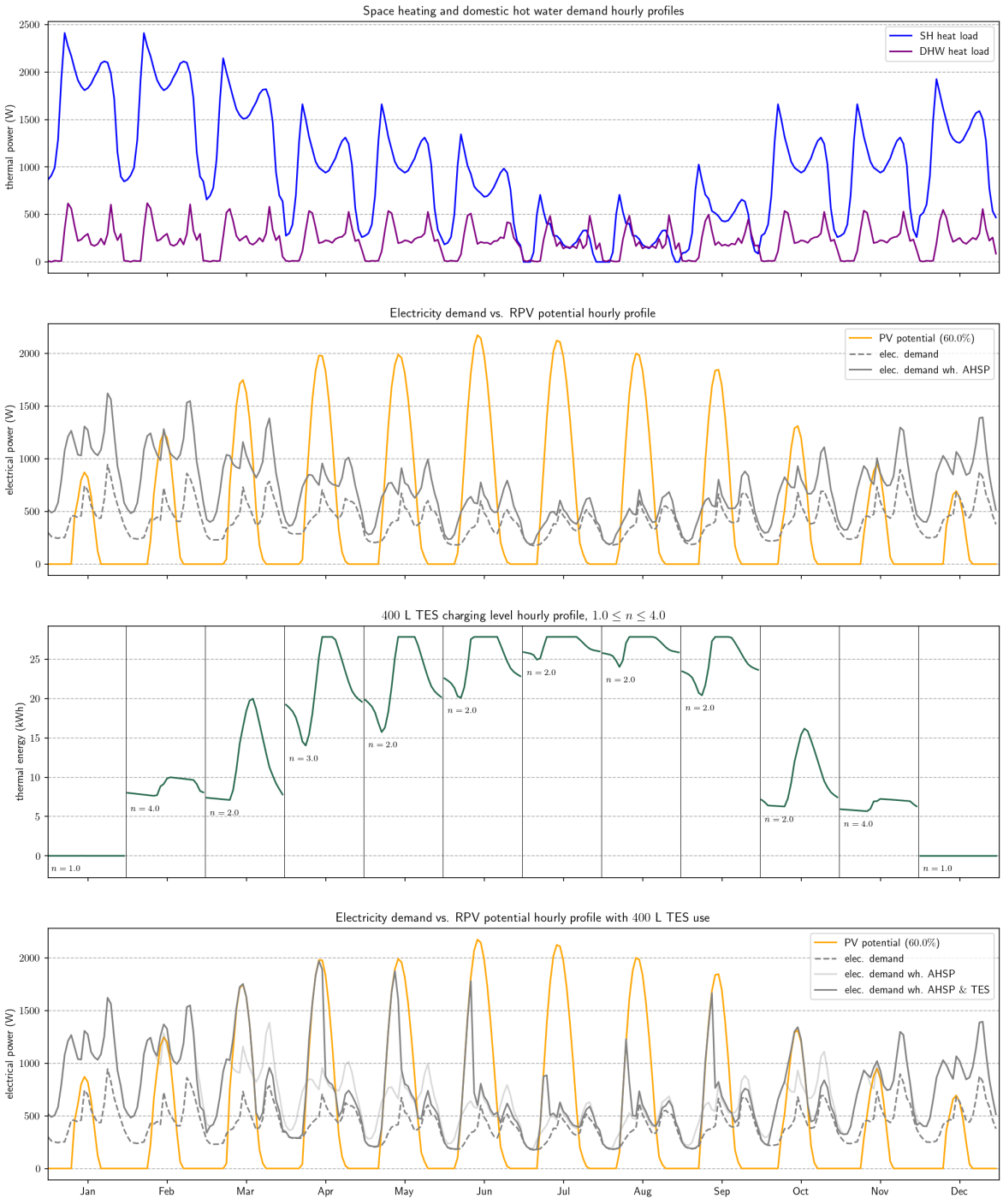


Figure 5: System operation visualization for RSF building with ASHP, 39.9 $m^2$ RPV surface, and 400 L TES capacity system configuration. (EGID : 1029179.)

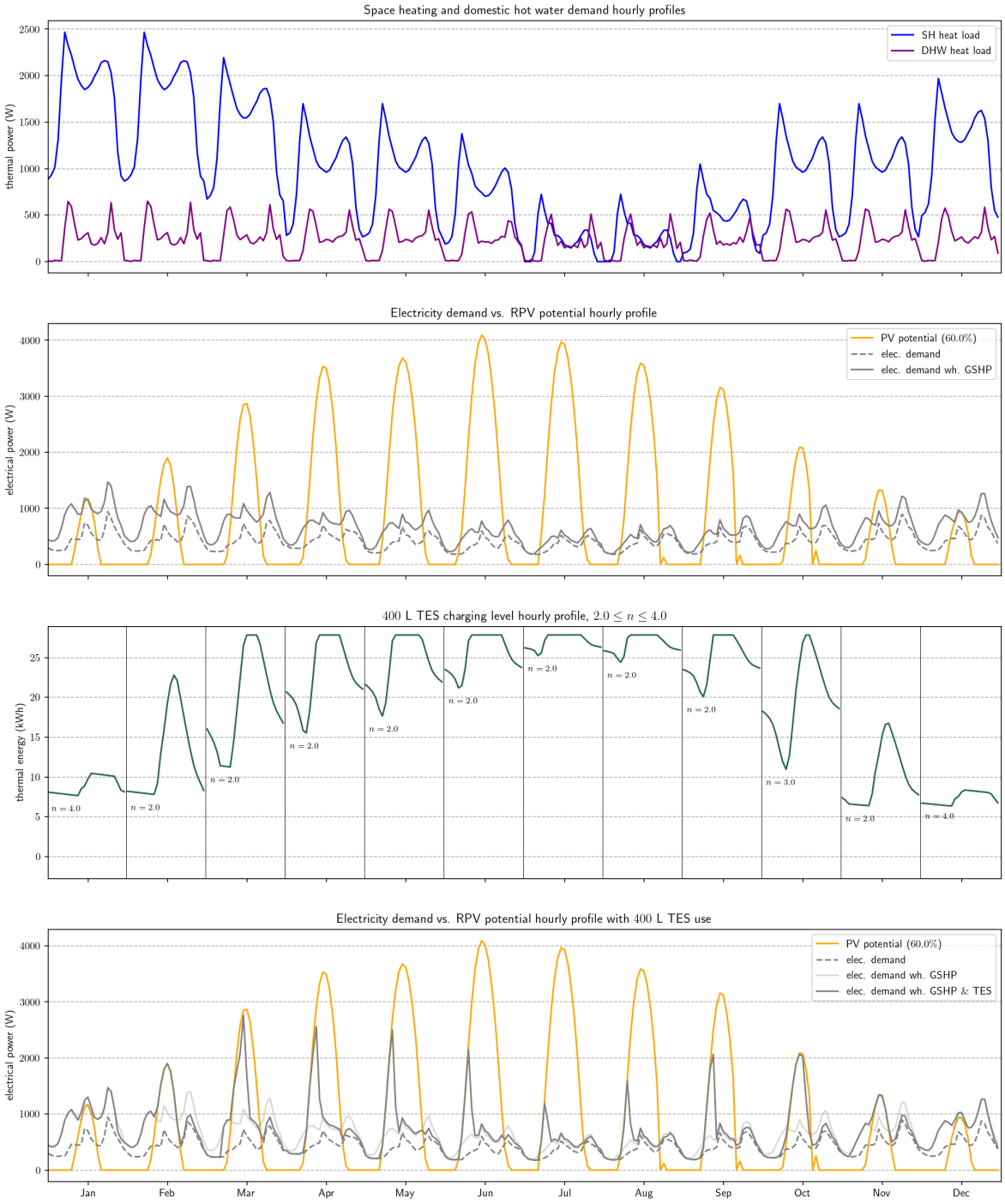


Figure 6: System operation visualization for RSF building with GSHP, 50.7 $m^2$ RPV surface, and 400 L TES capacity system configuration. (EGID : 1028823.)

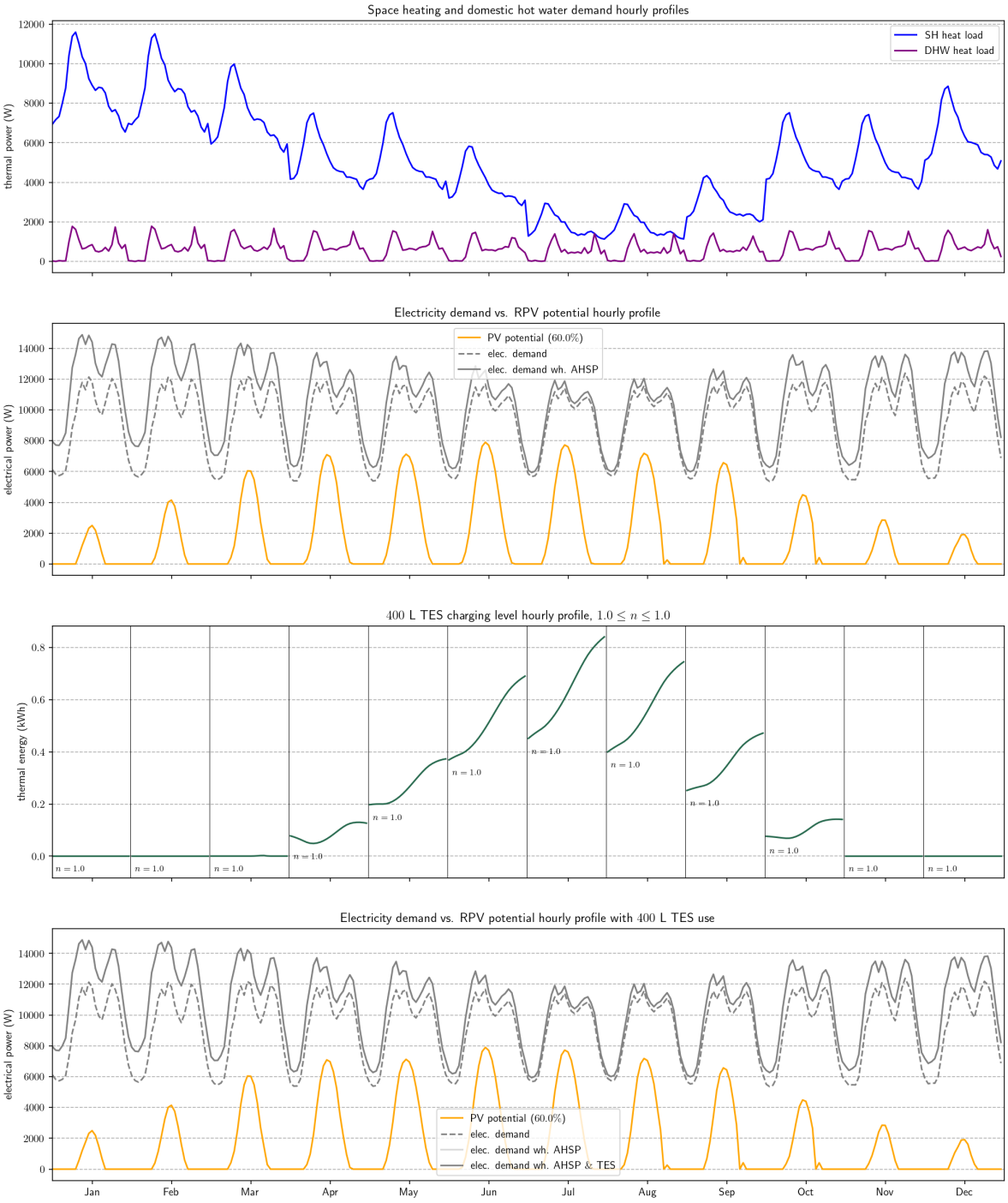


Figure 7: System operation visualization for SER building with ASHP, 119.6 $m^2$ RPV surface, and 400 L TES capacity system configuration. (EGID : 1029027.)

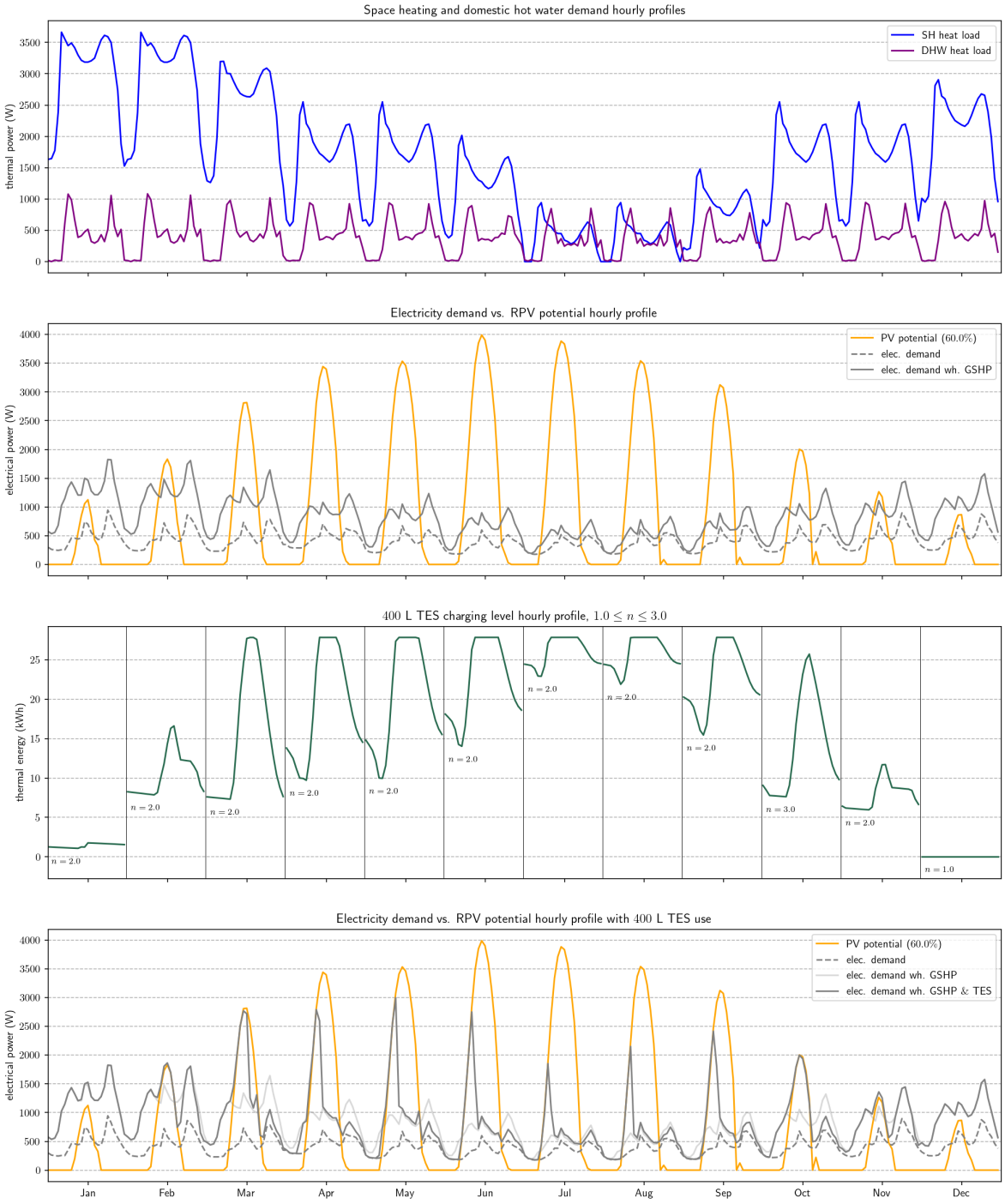


Figure 8: System operation visualization for RMF building with GSHP, 54.9 $m^2$ RPV surface, and 400 L TES capacity system configuration. (EGID : 1028854.)

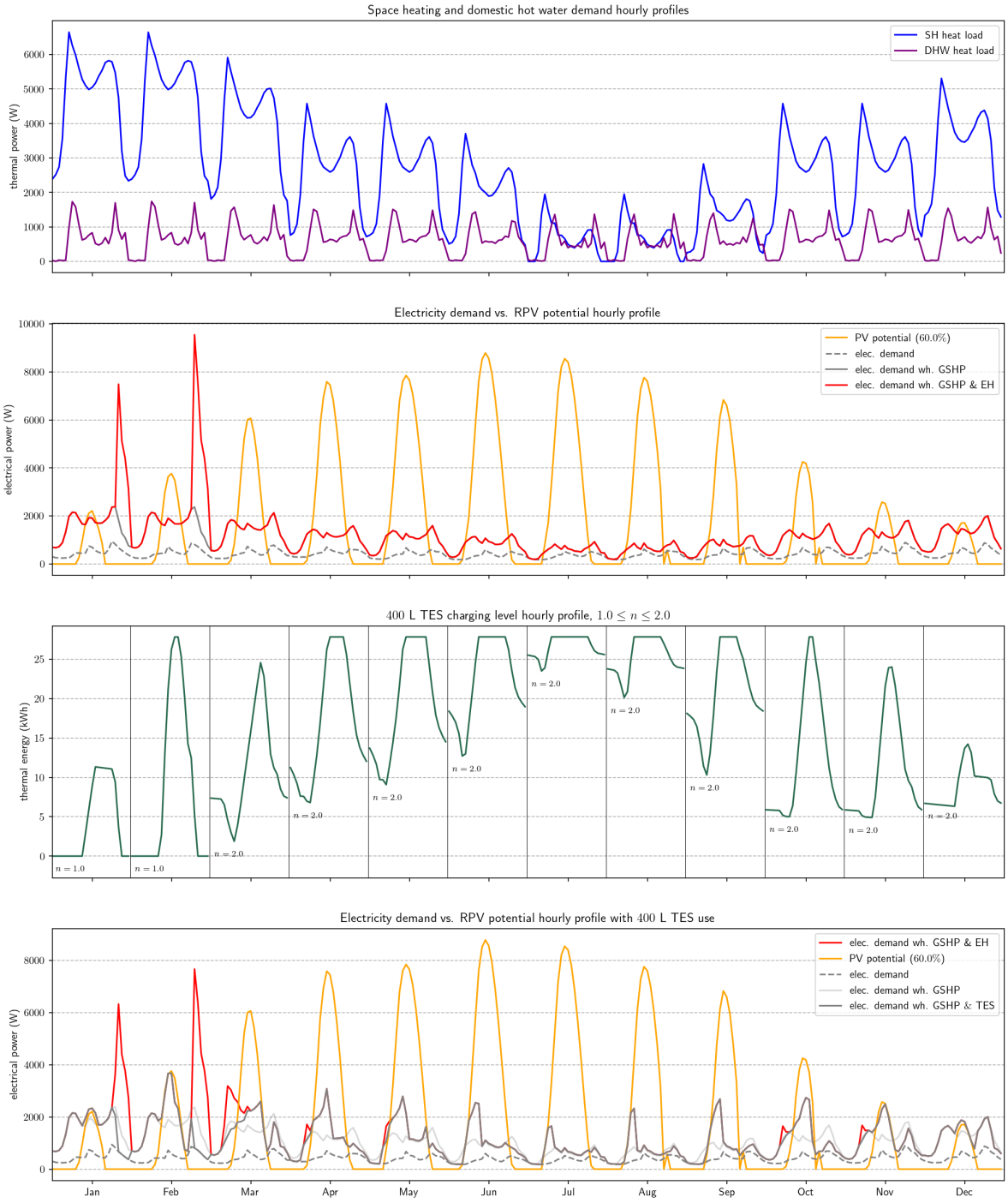


Figure 9: System operation visualization for RES building with GSHP, EH, 110.6 $m^2$ RPV surface, and 400 L TES capacity system configuration. (EGID : 1029232.)

## 6.2 Energy related performance

Previously defined indicators (see Sect. 3) are plotted for each building. The behaviour of the HRES is analysed depending on the available surface area of the RPV installation and TES capacity. Single indicator bi-dimensional plot charts are presented first so that the system performance can be related to each one of them. Then, linear combination proposed in 16 is used with the aim of sizing the optimal SPV installation and the storage tank.

### 6.2.1 Self-consumption ratio

Self-consumption ratio is not defined when the RPV surface area is nil, whatever the TES volume. This means the hatched rectangular area on the left hand side of each chart. Global evolution trend is the following : the lower the surface area, the higher the autonomy level is. Regarding the TES capacity, the higher the volume, the higher the autonomy level is. TES dependence is more important for lower volumes ($x_2 < 600$). On Fig. 12 , self-consumption ratio of RMF building is constant and equals to one because the electricity demand is always greater than domestic production.

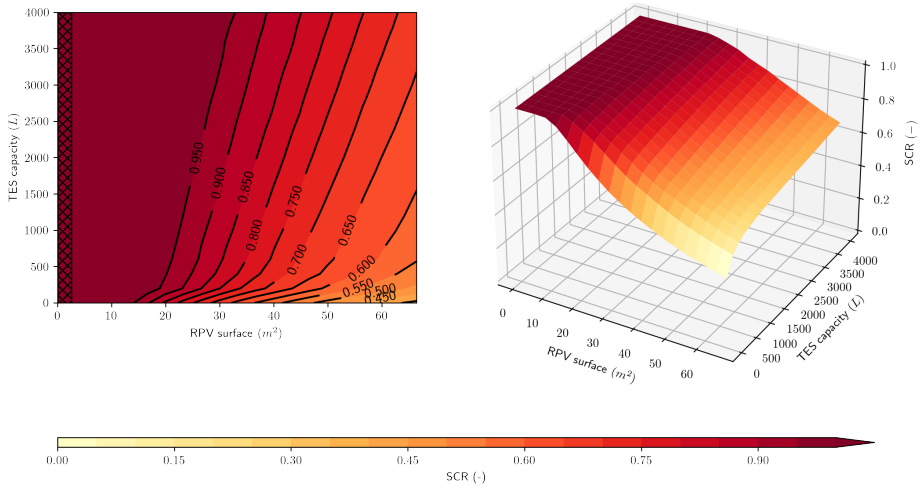


Figure 10: RPV surface and TES capacity dependence of self-consumption ratio for RSF building with ASHP. (EGID : 1029179.)

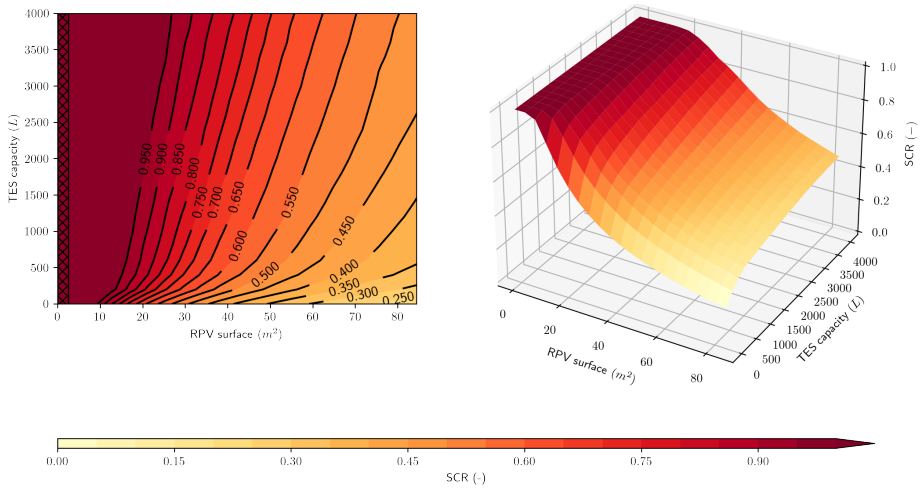


Figure 11: RPV surface and TES capacity dependence of self-consumption ratio for RSF building with GSHP. (EGID : 1028823.)

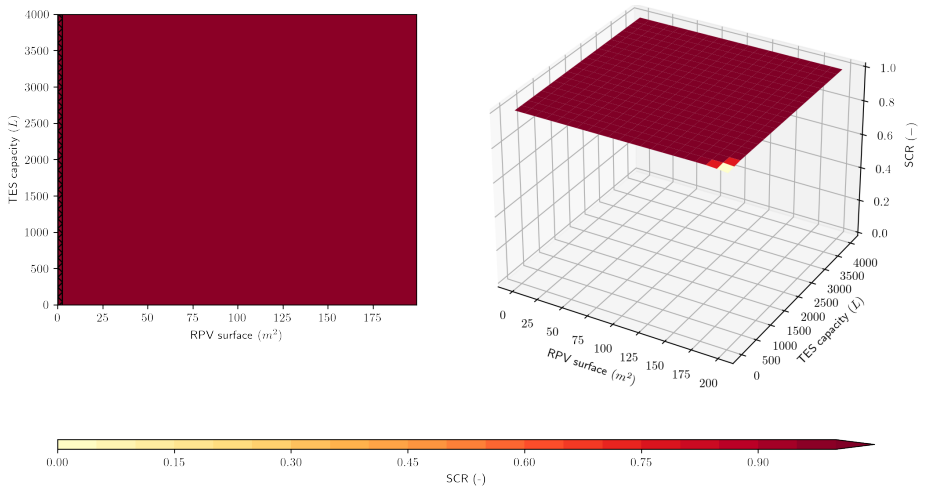


Figure 12: RPV surface and TES capacity dependence of self-consumption ratio for SER building with ASHP. (EGID : 1029027.)

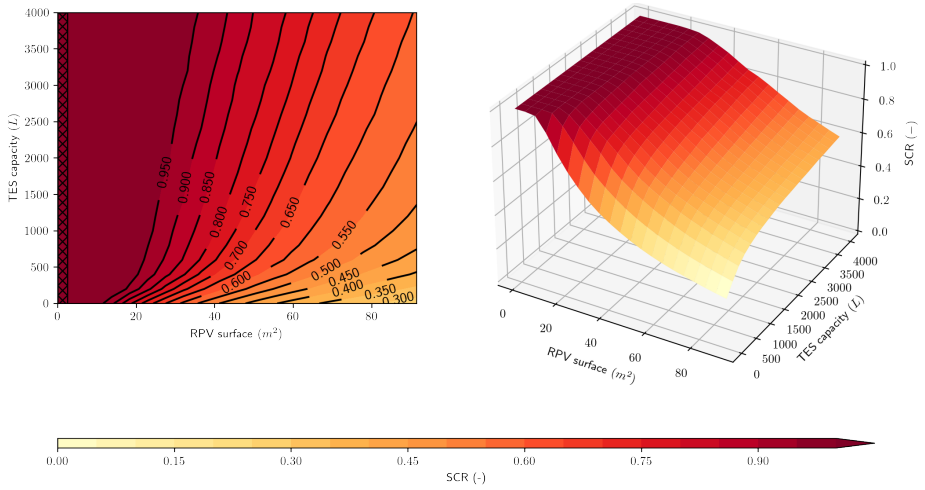


Figure 13: RPV surface and TES capacity dependence of self-consumption ratio for RMF building with GSHP. (EGID : 1028854.)

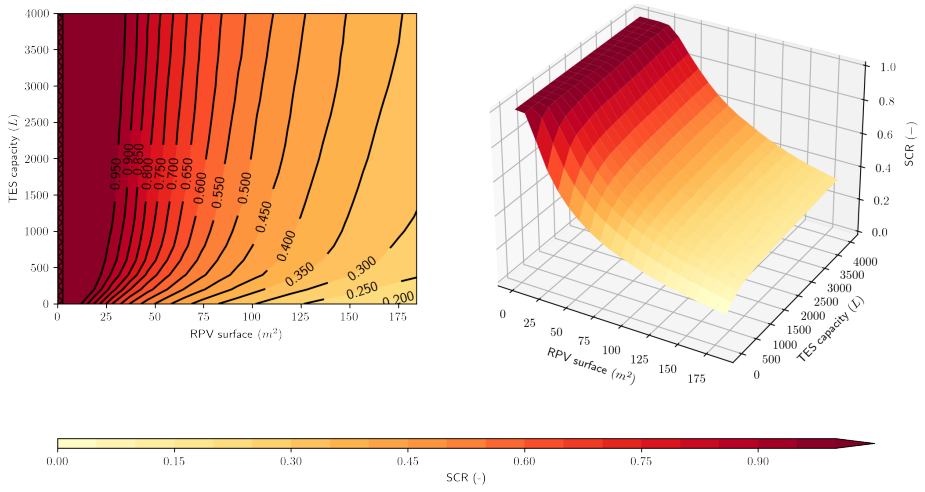


Figure 14: RPV surface and TES capacity dependence of self-consumption ratio for RSF building with GSHP. (EGID : 1029232.)

### 6.2.2 Self-sufficiency ratio

Self-sufficiency ratio increases with both the RPV surface area and TES capacity increase. Like for the self-consumption ratio, TES dependence is more important for lower volumes. On Fig. 17, we can observe self-sufficiency ratio of RMF building is not any TES dependence. The only variation of $E_L$ as indicator denominator is too slight to entail any visible self-sufficiency ratio variation.

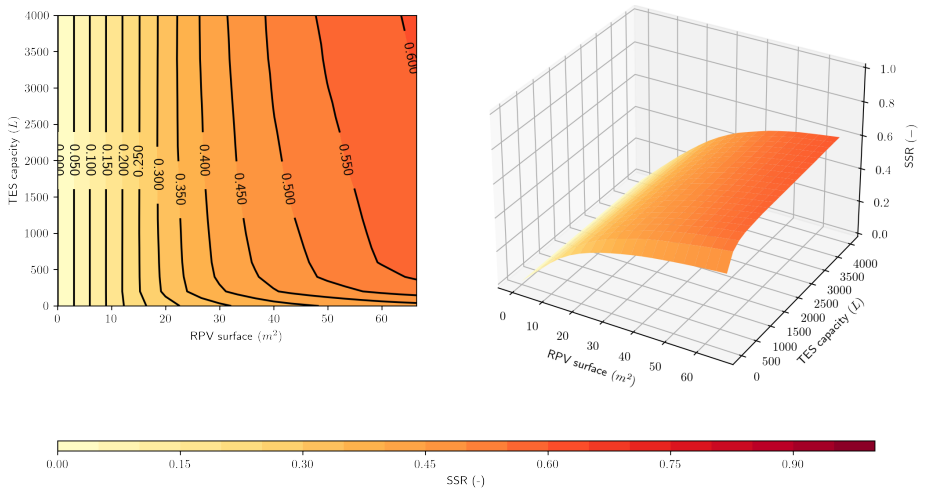


Figure 15: RPV surface and TES capacity dependence of self-sufficiency ratio for RSF building with ASHP. (EGID : 1029179.)

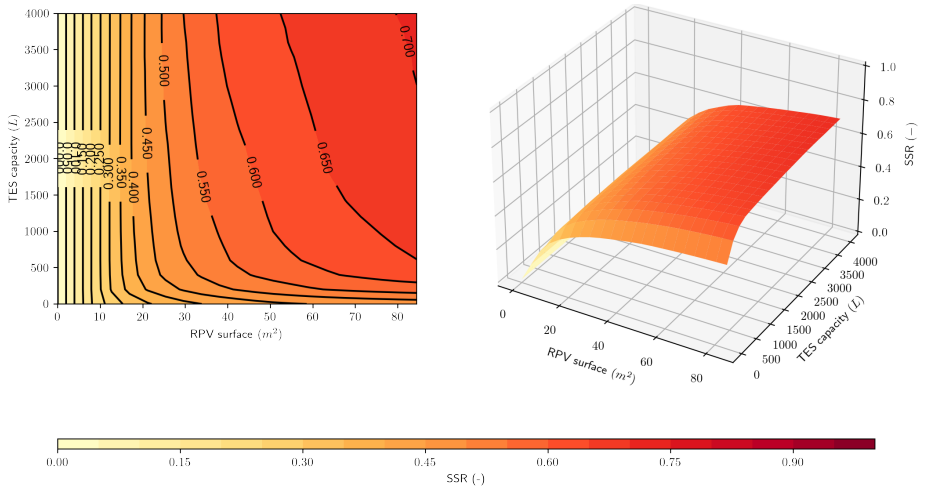


Figure 16: RPV surface and TES capacity dependence of self-sufficiency ratio for RSF building with GSHP. (EGID : 1028823.)

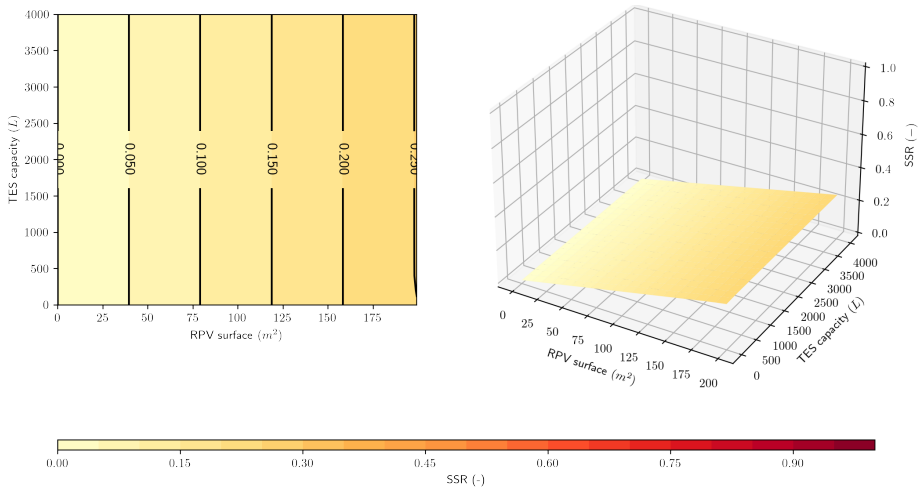


Figure 17: RPV surface and TES capacity dependence of self-sufficiency ratio for SER building with ASHP. (EGID : 1029027.)

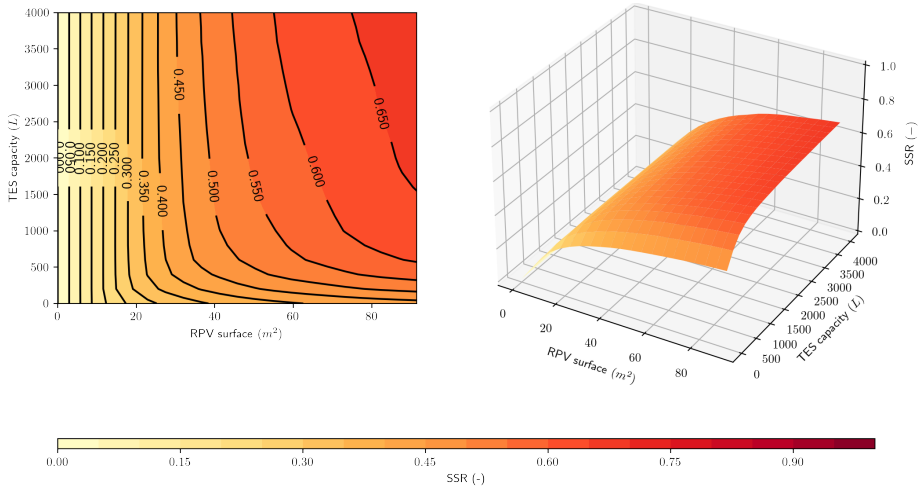


Figure 18: RPV surface and TES capacity dependence of self-sufficiency ratio for RMF building with GSHP. (EGID : 1028854.)

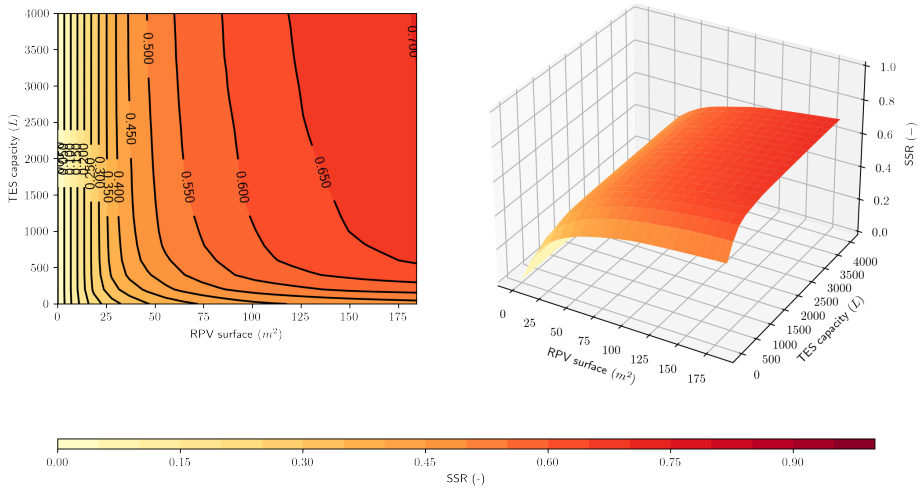


Figure 19: RPV surface and TES capacity dependence of self-sufficiency ratio for RSF building with GSHP and EH. (EGID : 1029232.)

### 6.2.3 Grid based electricity use performance factor

Grid based electricity use performance factor enables to count grid electricity saving compared to the reference case, that is without any storage use. Indicator evolution on $A_{PV} \times V_{TES}$ cannot be easily apprehended due to temperature condition inclusion during TES discharging operation. The indicator is constant on Fig. 22 whatever $x_1 \in A_{PV}$ and $x_2 \in V_{TES}$. So, there is no gain in terms of energy saving in comparison with the reference case.

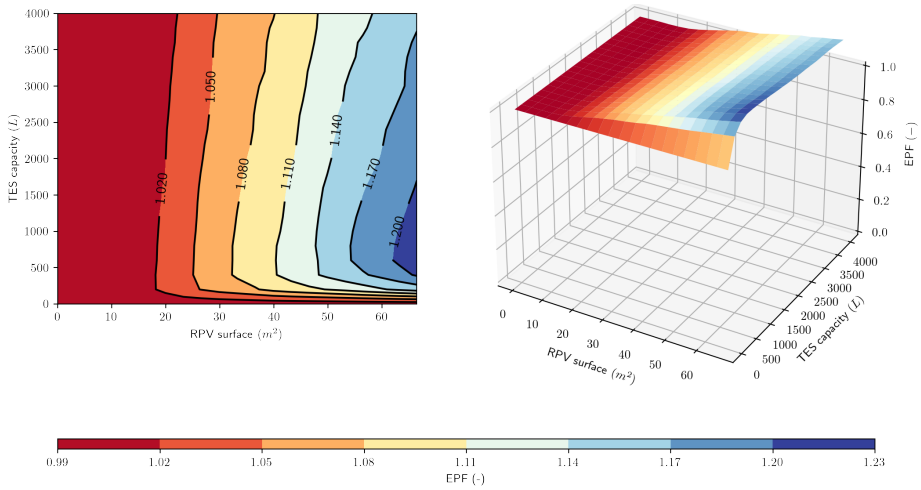


Figure 20: RPV surface and TES capacity dependence of grid based electricity use performance factor for RSF building with ASHP. (EGID : 1029179.)

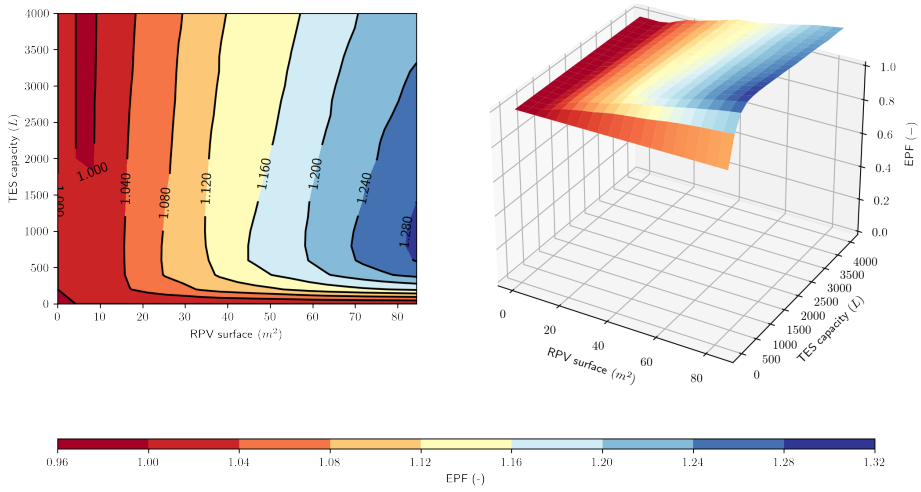


Figure 21: RPV surface and TES capacity dependence of grid based electricity use performance factor for RSF building with GSHP. (EGID : 1028823.)

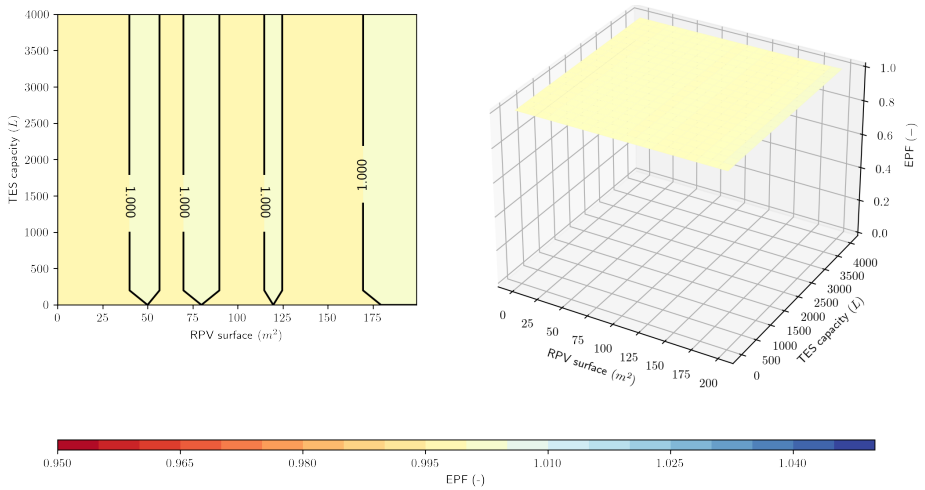


Figure 22: RPV surface and TES capacity dependence of grid based electricity use performance factor for SER building with ASHP. (EGID : 1029027.)

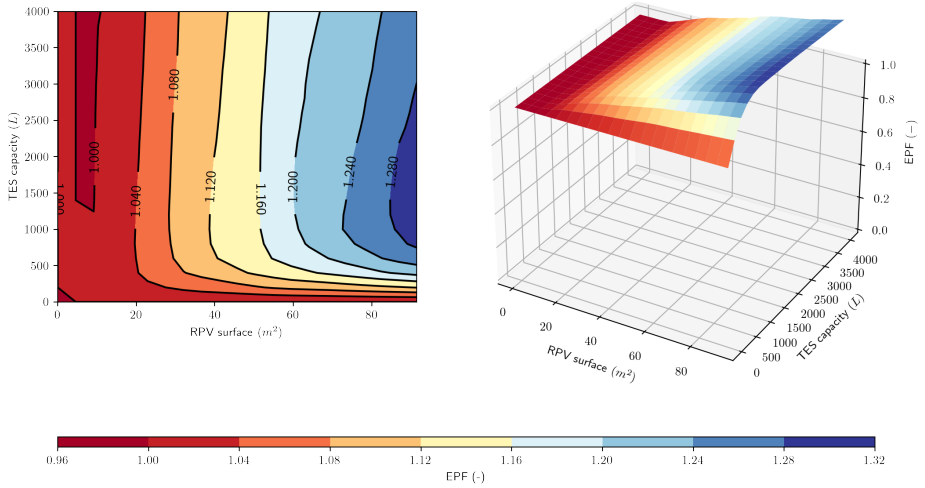


Figure 23: RPV surface and TES capacity dependence of grid based electricity use performance factor for RMF building with GSHP. (EGID : 1028854.)

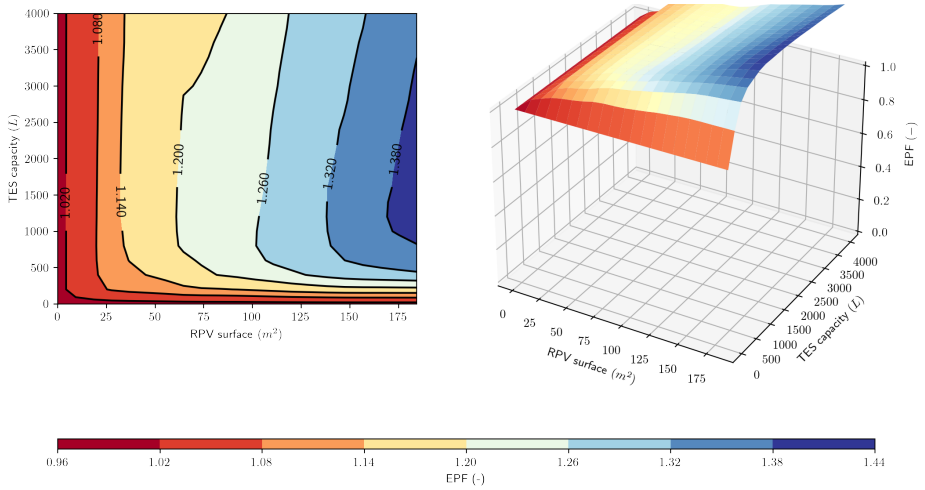


Figure 24: RPV surface and TES capacity dependence of grid based electricity use performance factor for RSF building with GSHP and EH. (EGID : 1029232.)

## 6.3 Optimization

### 6.3.1 Objective space

The $y$ variable is plotted depending on available surface of the RPV installation and TES capacity. On each chart, magenta triangle shows the maximum value obtained. Optimal surface of RPV installation matches the maximum available surface for all buildings. Basically, energy performance of distributed HRES could be higher with greater RPV surface area at building level. This can be explained from low roof surface over energy demand surface ratio. Optimal TES capacity is in range $0-4000\,L$. On Fig. 27, we can note normalization procedure and plot resolution allow to reach a maximum. In spite of weak meaning of related key indicators taken separately, objective space admits a maximum. We can also note the heat demand is much higher than for most of the RSF and RMF buildings. In addition, the temperature condition implies the optimal TES capacity found is large enough.

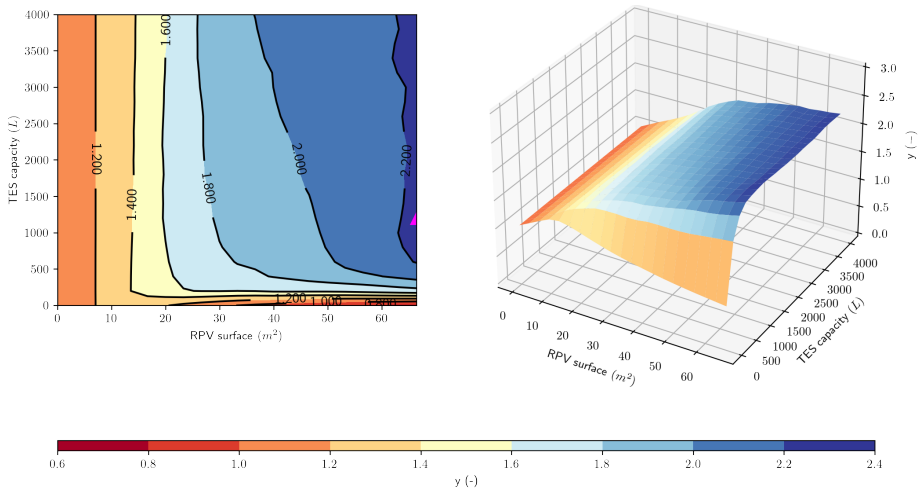


Figure 25: RPV surface and TES capacity dependence of $y$ objective variable for RSF building with ASHP. (EGID : 1029179.)

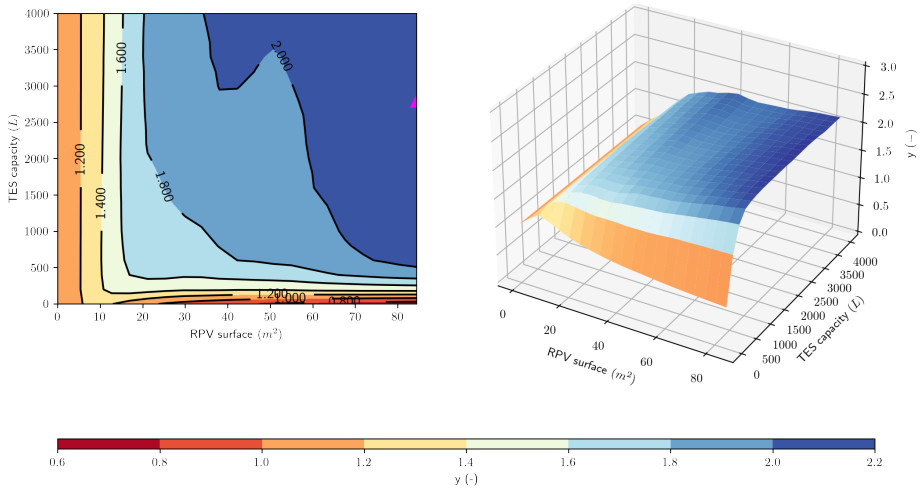


Figure 26: RPV surface and TES capacity dependence of $y$ objective variable for RSF building with GSHP. (EGID : 1028823.)

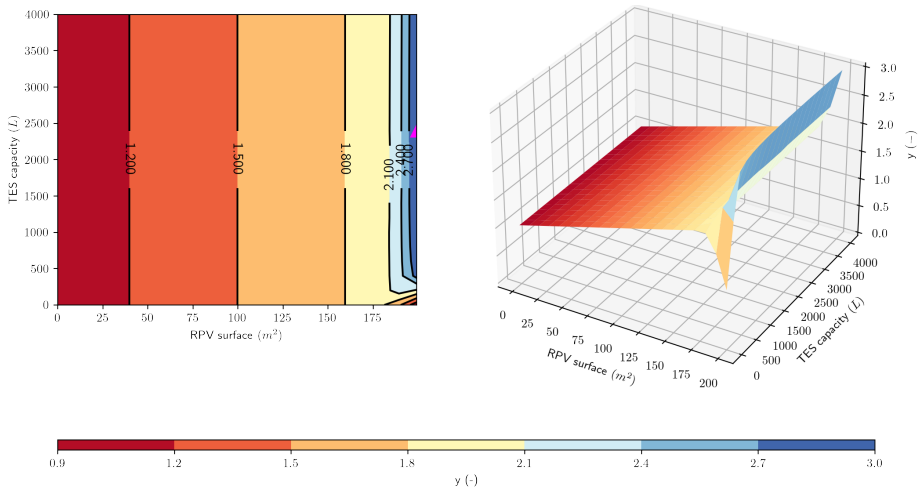


Figure 27: RPV surface and TES capacity dependence of $y$ objective variable for SER building with ASHP. (EGID : 1029027.)

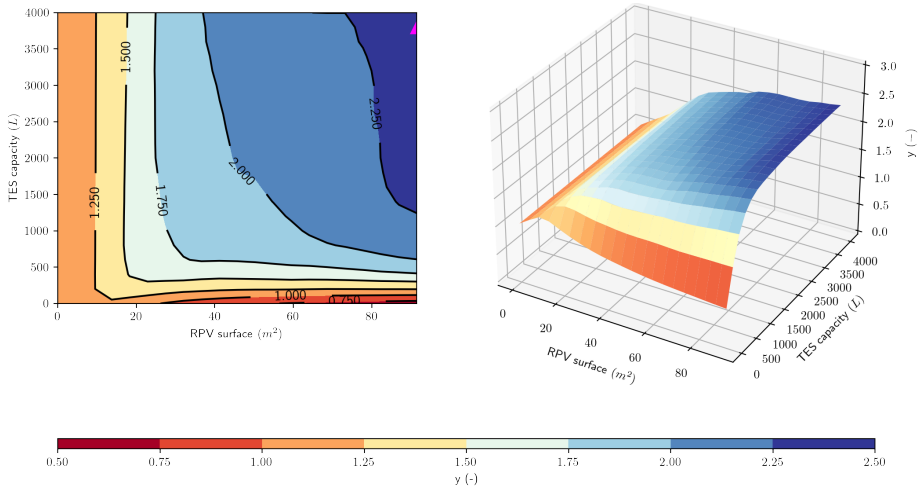


Figure 28: RPV surface and TES capacity dependence of $y$ objective variable for RMF building with GSHP. (EGID : 1028854.)

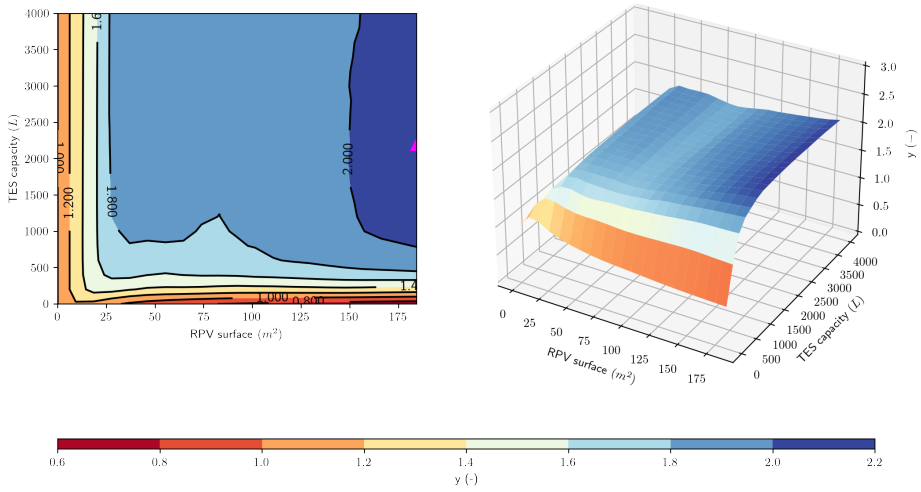


Figure 29: RPV surface and TES capacity dependence of $y$ objective variable for RSF building with GSHP and EH. (EGID : 1029232.)

Optimal sizing based on value $J = \max\{y \in [0, 3] \,|\, x_1 \in S_{PV}, x_2 \in V_{TES}\}$ for the five buildings is presented in Table 4.

| EGID | 1029179 | 1028823 | 1029027 | 1028854 | 1029232 |
|---|---|---|---|---|---|
| RPV surface ($m^2$) | 66.5 | 84.5 | 199.4 | 91.5 | 184.4 |
| TES capacity ($L$) | 1 200 | 2 800 | 2 400 | 3 800 | 2 200 |
| SCR | 0.589 | 0.415 | 1.000 | 0.574 | 0.315 |
| SSR | 0.584 | 0.681 | 0.252 | 0.673 | 0.692 |
| EPF | 1.212 | 1.272 | 1.003 | 1.277 | 1.401 |

Table 4: HRES equipment sizing proposition based on $J$ variable.

### 6.3.2 Optimal sizing

Data and algorithm output signal are plotted again based on sizing parameters found. For all the buildings, a new reference case is defined according to the RPV surface installation selected based on the optimization procedure seen before. This matches 100 % of the available surface for all the buildings. The idea behind the optimization procedure is to timely match electricity demand with RPV potential thanks to the use of TES. Since the heat demand profiles are different depending on each month, the main objective is thus to find ideal yearly configuration.

Some conclusions can be applicable for all the buildings. Although it is never performed on a full capacity range, usage of TES is maximal during the intermediate season. Temperature condition forces to store minimum energy prior to make TES discharging operation possible. Moreover, a charging level profile pattern is often observable on the whole year. This roughly matches the RPV potential yearly pattern. Since the storage charging operation is based on the electricity excess power supply, the maximum charging level is obtained during summer period and the minimum level during winter period. Furthermore, RPV potential during winter and intermediate seasons seems to be decisive for sizing procedure.

Since the two RSF buildings shown in Fig. 30 and Fig. 31 have close features in terms of energy demand and potential, their results can be compared. The use of ASHP in the first building still drives overall larger electricity demand. As a consequence, yearly self-consumption ratio indicator reaches higher value with ASHP utilization but self-sufficiency ratio and grid based electricity used performance factor reach higher values with GSHP utilization. Storage charging level reaches its maximum value eight over twelve months for both two buildings. The maximum number of days necessary to reach quasi-permanent condition is 14 in the first case and 24 in the second one. It appears during March month in both cases. Finally, RPV potential is greater in the second case than in the first one due to larger roof surface available. This leads to better performance, during the months November, December, and February especially. On the whole year, the HRES related to Fig. 31 allows to save more than 27 % of grid-based electricity (in comparison with the reference case) against about 21 % for the HRES related to Fig. 30 .

Results regarding the SER building in Fig. 32 are more specific. Due to much lower roof surface over floor surface ratio compared to residential buildings, the RPV potential is lower than the electricity demand the most of the time over the year. Therefore, self-consumption ratio reaches the value 1. Sizing procedure leads to select a reservoir which may seem large enough. However, the heat demand is important also. The use of TES enables to slightly lower electricity demand for heating over the period from June to August only.

We can see in Fig. 33, the highest heat demand among the RSF buildings drives the largest storage capacity selection. It allows time extended GSHP operation during sunny period. However, RPV potential does not allow to save any grid-based

electrical energy during December and January months.

Interpretation of charts in Fig. 34 is more complicated due to EH additional use. It leads to best performances in terms of self-sufficiency and grid-based electricity saving. In spite of this observation, a large part of RPV production is not used ; self-consumption ratio reaches the minimum value among all the three buildings.

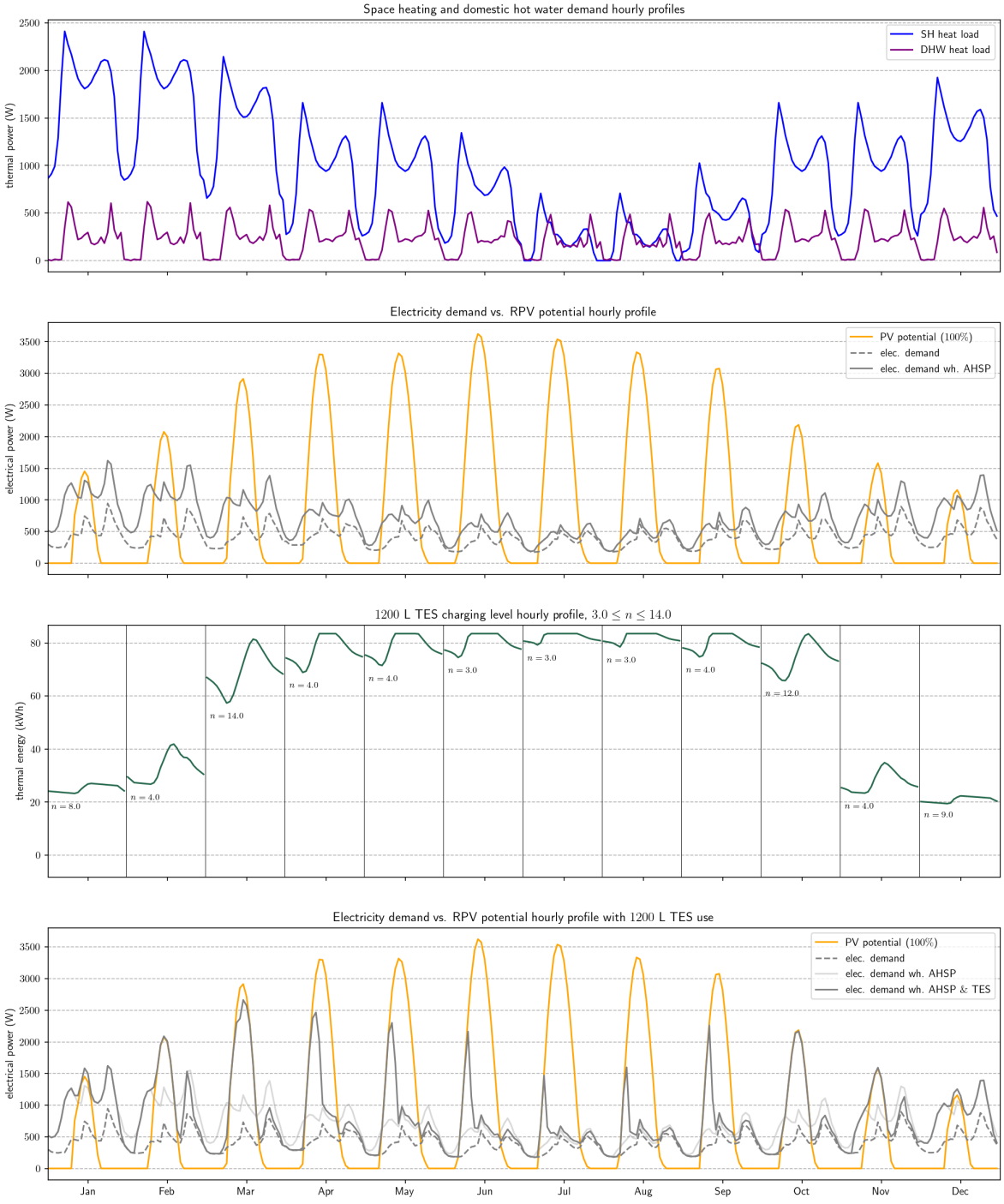


Figure 30: System operation visualization for RSF building with ASHP, 66.5 $m^2$ RPV surface and 1 200 L TES capacity system configuration. (EGID : 1029179.)

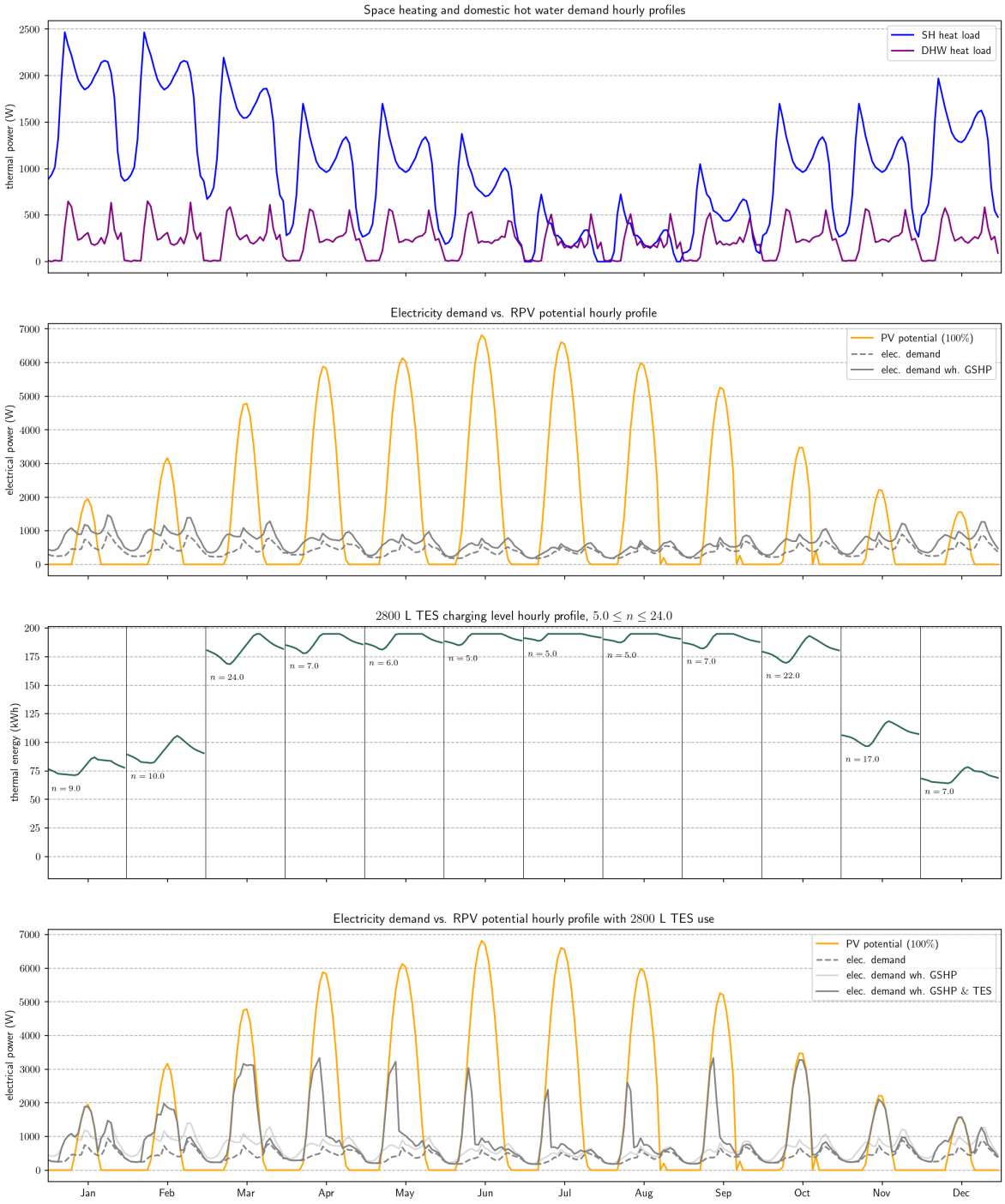


Figure 31: System operation visualization for RSF building with GSHP, 84.5 $m^2$ RPV surface and 2 800 L TES capacity system configuration. (EGID : 1028823.)

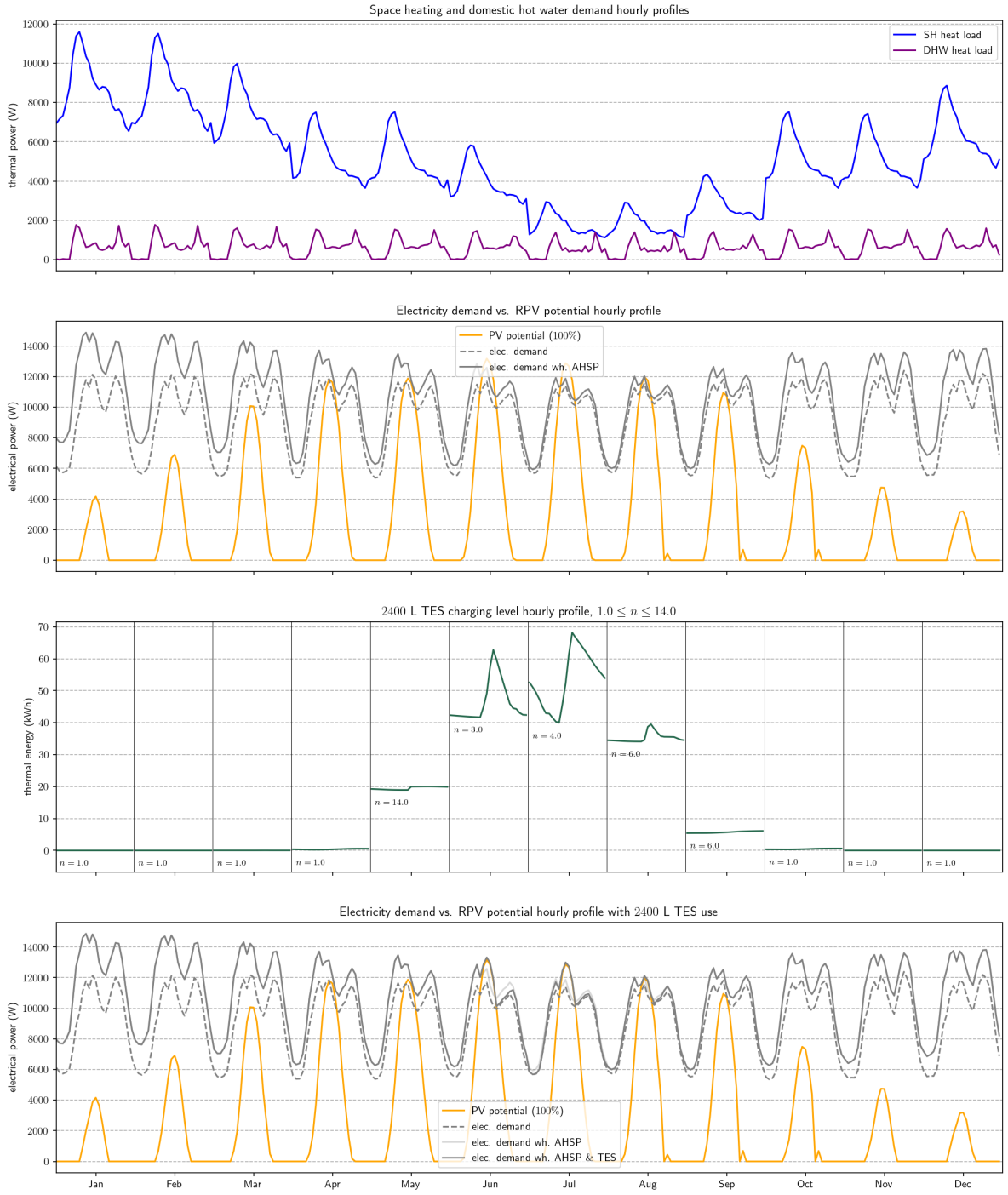


Figure 32: System operation visualization for SER building with ASHP, 199.4 $m^2$ RPV surface, and 2 400 L TES capacity system configuration. (EGID : 1029027.)

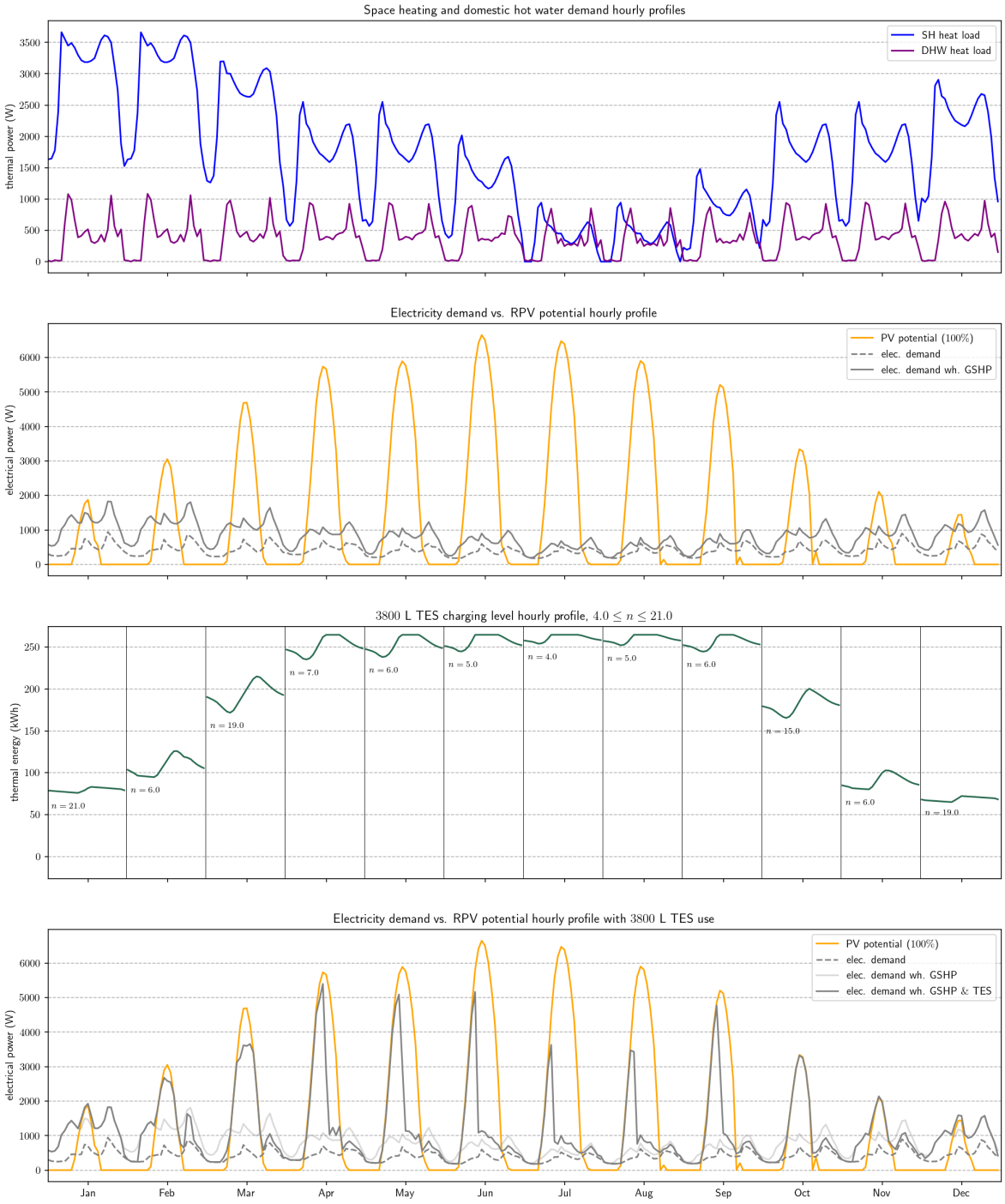


Figure 33: System operation visualization for RMF building with GSHP, 91.5 $m^2$ RPV surface, and 3 800 L TES capacity system configuration. (EGID : 1028854.)

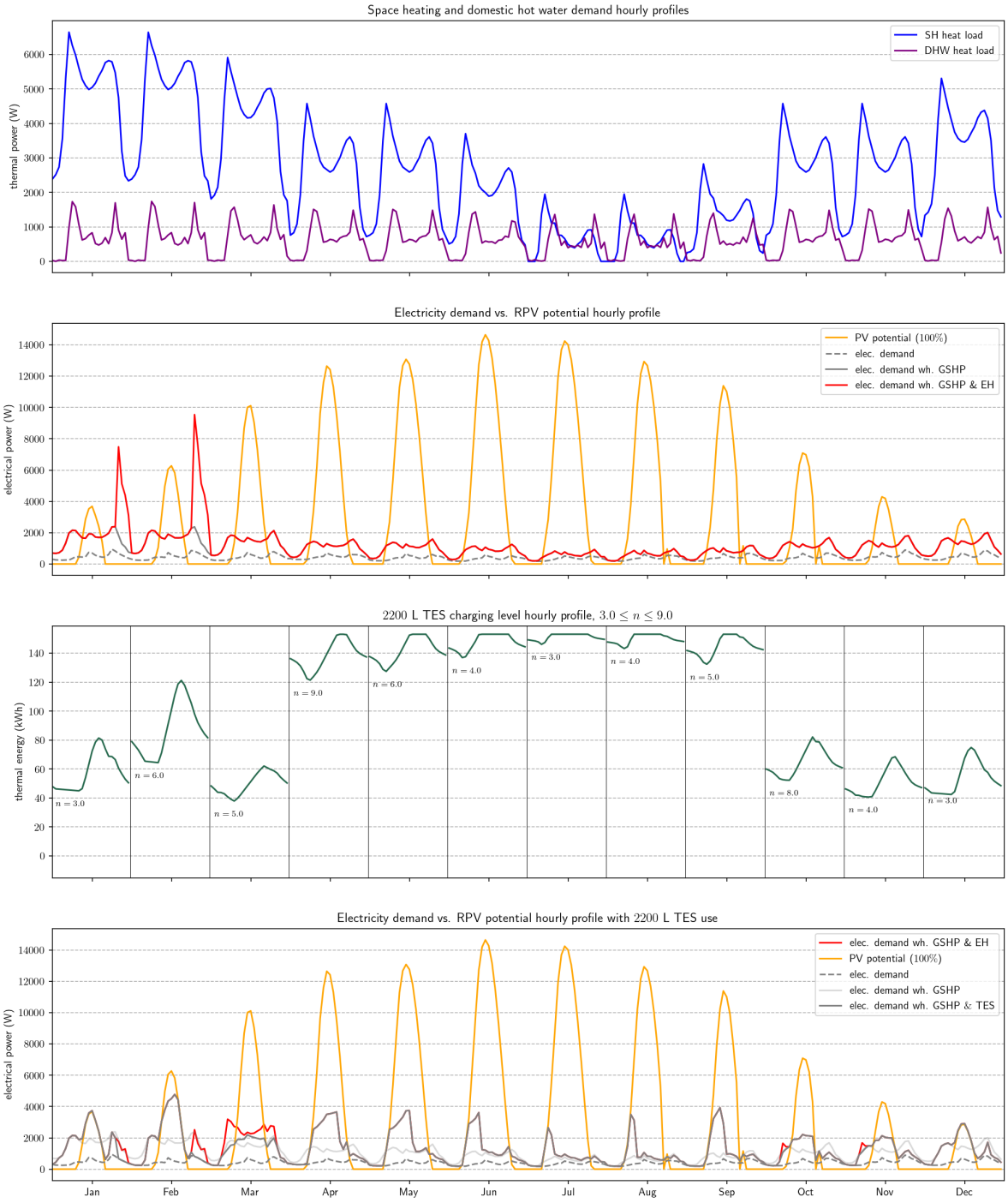


Figure 34: System operation visualization for RSF building with GSHP, EH, 184.4 $m^2$ RPV surface, and 2 200 L TES capacity system configuration. (EGID : 1029232.)

# 7 Conclusion

It has been shown the strategy to combine HP with RPV installation was relevant. The possible increase in self-consumption of photovoltaic electricity by the use of TES has been achieved following two mechanisms : (i) the electricity demand was increased for storage charging when hourly net SPV production was positive, (ii) it was decreased thanks to storage discharging when hourly net SPV production was negative. A control algorithm has been specifically developed to this end. Physical limit as temperature of carrying fluid condition has been accounted for preventing system performance assessment from misleading. The procedure followed in the present work is easily generalizable. It needs low computational resource. This does not need very specific building related information to be applicable. The procedure has been tested on case study covering an area at urban scale. The Fig. 35 shows the specific location of covered buildings in the present work with their corresponding self-consumption and self-sufficiency ratio indicators obtained. From the left hand to the right hand side, there are the buildings identified with the EGID number 1 028 854, 1 029 232, 1 028 823 (at the bottom), then 1 029 027, and finally the building identified 1 029 179. An extended application to a much larger area would be possible without having to face a great complexity increase.

An optimization task has been approached as sizing problem. For this, SPV self-sufficiency has been first monitored in addition to the self-consumption. The indicator has enabled to counterbalance the downsizing trend due to self-consumption ratio definition regarding the surface of RPV installation. This latter matches the maximum RPV installation surface for each building. Therefore, it does not seem to be a relevant indicator suited this kind of energy performance optimization problem. To have at disposal larger installation surface would allow to know if the objective function has got extremum surface area dependent. A third indicator has been monitored moreover : grid-based electricity use performance factor. This quantified the electricity saving in comparison to the case without any TES equipment. This has enabled to limit the daily storage size as much as possible. Other considerations would need to be taken into account in the practical case such as the available space in each specific building for TES installation or the additional cost it involves.

The data is formatted in MMH. For each monthly typical day, the day+$n$ does not strictly present same energy potential any more. Monthly daily repetition of TES charging and discharging operation could be improved by an additional statistical approach. This to account the effect of the operation repetition on the RPV hourly production and thus reinforce the model reliability.

The control algorithm has been developed for TES charging and discharging operations at single building scale only. During summer and a large part of intermediate season near the summer (before or after), a large SPV potential remains unused for the residential buildings. To centralize operation control at larger scale would present benefits for a better RES integration to the grid by complying HRES to grid curtailment. Several buildings could be grouped by electricity consumers community and take part in an energy sharing management process. A specific building arrangement would be to find out. This could still improve the global energy performance on the area. In short, a such HRES may represent a great potential as operating reserve for the utilities.

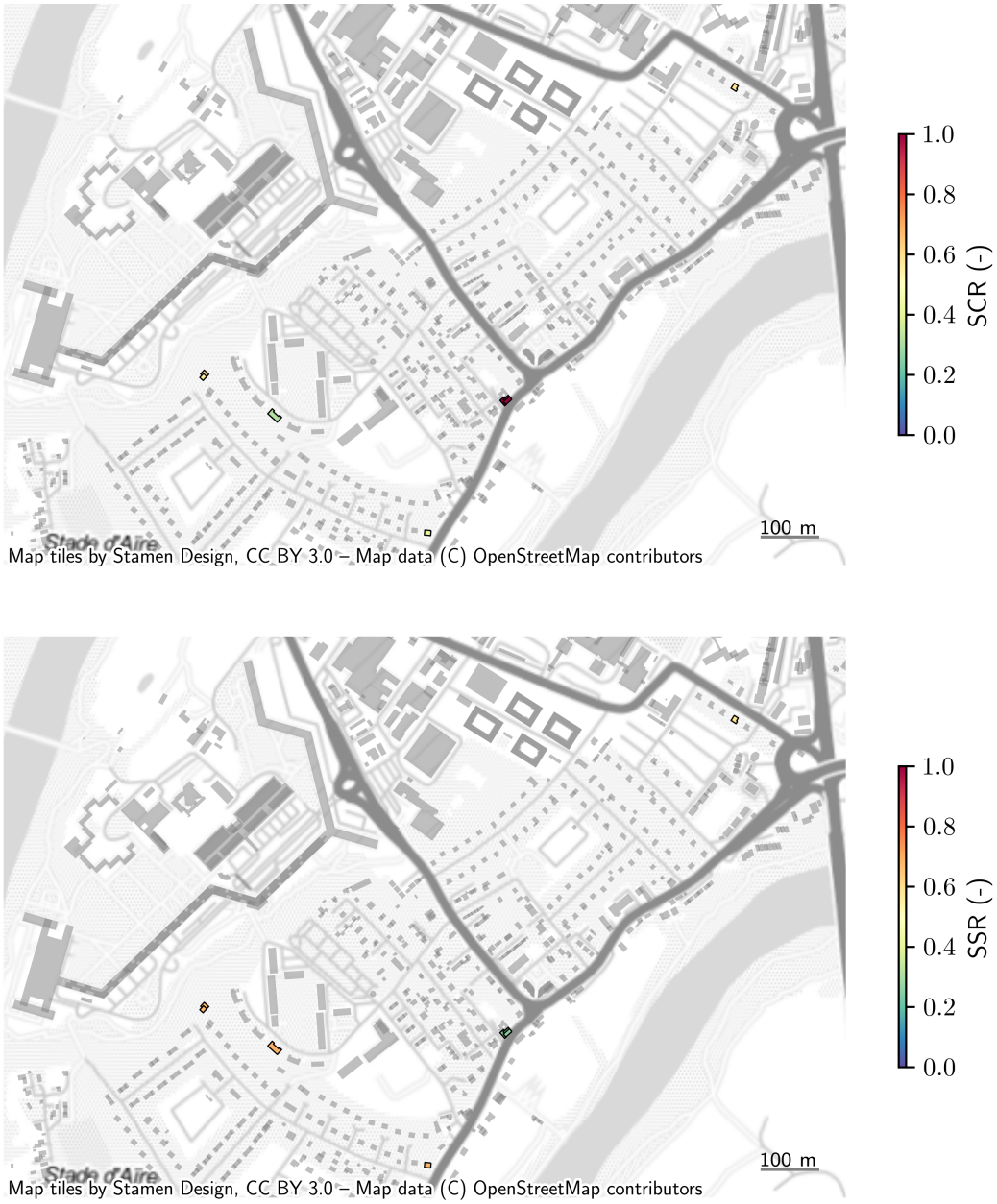


Figure 35: Location map of the five buildings considered with their self-consumption ratio, on the top, and their self-sufficiency ratio, at the bottom.

# Appendix A - Supply and return temperatures calculation

Let consider the whole heating system of a given building as a counterflow exchanger between carrying fluid and ambient air within the room. Whatever the kind of heating system (radiator, heating floor, etc.), we know the heat transfer can be calculated from (7). So, we have :

$$\dot{Q} = K_{rad} \frac{[(T_{sup} - T_{room}) - (T_{ret} - T_{room,0})]^n}{\ln^n \left( \frac{T_{sup} - T_{room}}{T_{ret} - T_{room,0}} \right)}$$

Since both members are positives, we can write :

$$\ln \left( n \ln \left( \frac{T_{sup} - T_{room}}{T_{ret} - T_{room,0}} \right) \right) = \ln \left( \frac{K_{rad}}{\dot{Q}} \right) + n \ln[(T_{sup} - T_{room}) - (T_{ret} - T_{room,0})]$$

This yields to :

$$\frac{T_{sup} - T_{room}}{T_{ret} - T_{room,0}} = \exp \left[ \left( \frac{K_{rad}}{\dot{Q}} \right)^{1/n} ((T_{sup} - T_{room}) - (T_{ret} - T_{room,0})) \right]$$

Then, we can write :

$$\begin{aligned} T_{ret} - T_{room,0} &= \frac{T_{sup} - T_{room}}{\exp \left[ \left( \frac{K_{rad}}{\dot{Q}} \right)^{1/n} ((T_{sup} - T_{room}) - (T_{ret} - T_{room,0})) \right]} \\ &= \frac{T_{sup} - T_{room} - (T_{ret} - T_{room,0})}{\exp \left[ \left( \frac{K_{rad}}{\dot{Q}} \right)^{1/n} ((T_{sup} - T_{room}) - (T_{ret} - T_{room,0})) \right] \left( 1 - \frac{T_{ret} - T_{room,0}}{T_{sup} - T_{room}} \right)} \\ &= \frac{T_{sup} - T_{ret} - (T_{room} - T_{room,0})}{\exp \left[ \left( \frac{K_{rad}}{\dot{Q}} \right)^{1/n} ((T_{sup} - T_{room}) - (T_{ret} - T_{room,0})) \right] - 1} \end{aligned}$$

Furthermore, since the heating control strategy is supposed to be temperature dependant and constant flow rate, we can write also :

$$\dot{Q} = \dot{m} c_p (T_{sup} - T_{ret})$$

The heat load is fed to the ambient air within the local and we have $\dot{Q} = \dot{m}_{air} c_{p_{air}} (T_{room} - T_{room,0})$. Let suppose $T_{room} \sim T_{room,0}$ and so $T_{room} - T_{room,0} \sim 0$. We can note this condition drives $\dot{m}_{air} = \frac{\dot{Q}}{c_{p_{air}} (T_{room} - T_{room,0})} \xrightarrow[T_{room} \to T_{room,0}]{} +\infty$. This being realistic. Finally, we get :

$$T_{ret} - T_{room} = \frac{\frac{\dot{Q}}{\dot{m} c_p}}{\exp \left( K_{rad}^{1/n} \dot{Q}^{1-1/n} \frac{1}{\dot{m} c_p} \right) - 1} = f_n(\dot{Q})$$

# Appendix B - Control algorithm

For a given time step, the following algorithm is applied to shift heat load. As a result, sought goal is to decrease electricity demand from the utility. The two types of heat demand are computed one by one and summed together at the end of the procedure. The algorithm is inserted in a specific loop so that the repetition is performed every 24 hours until quasi-permanent state condition is obtained.

**Algorithm 1:** TES charging and discharging control for space heating demand only.

**Require:** $Q_{SH}$, $Q_{DHW}$, $T_{SH}$, $Q_{HP}^{max}$, $E_{app}$, $E_{PV}$, $E_{HP}^{max}$, $Q_{TES}$, $Q_{TES}^{max}$, $T_{TES}$, $T_{source}$, $T_{ext}$, $T_{source} \in \mathbb{R}$

**Require:** $f_{COP} : \mathbb{R}_+ \to \mathbb{R}_+$

{TES losses calculation.}

$Q_{TES}^{loss} = b\,UA(T_{ext} - T_{TES})$

{Calculation of heat available from TES.}

$Q_{TES \to SH} = \max\{C_p(T_{TES} - T_{SH}), 0\}$

{Upper and lower HP operation boundaries.}

$Q_{HP,lower} = \max\{Q_{SH} - Q_{TES \to SH}, 0\}$

$Q_{HP,upper} = \min\{Q_{SH} + (Q_{TES}^{max} - Q_{TES}), Q_{HP}^{max}\}$

{Excess PV production and PV based heat production (thanks to the HP).}

$COP_{TES} = f_{COP}(T_{TES} - T_{source})$ {COP is $\Delta T_{source}^{sink}$ dependent. Calculation is performed from an external function $f_{COP}$}

$E_{PV^+} = \max\{E_{PV} - E_{app}, 0\}$

$Q_{PV^+} = E_{PV^+} \cdot COP_{TES}$

{TES charging level update.}

$Q_{HP} = \min\{Q_{HP,upper}, \max\{Q_{PV^+}, Q_{HP,lower}\}\}$

$\Delta Q_{TES} = Q_{HP} - Q_{SH} + Q_{TES}^{loss}$

$Q_{TES} = \max\{Q_{TES} + \Delta Q_{TES}, 0\}$

{HP operation control.}

$S = \frac{|Q_{TES}|}{Q_{TES}}$

$COP_{SH} = f_{COP}(T_{SH} - T_{source})$

$E_{HP,SH} = \frac{Q_{SH}}{COP_{SH}} + (\Delta Q_{TES} - Q_{TES}^{loss})\frac{S-1}{-2COP_{SH}} + (\Delta Q_{TES} - Q_{TES}^{loss})\frac{S+1}{2COP_{TES}}$

**return** $E_{HP,SH}$, $Q_{TES}$, $T_{TES}$

**Algorithm 2:** TES charging and discharging control for domestic hot water demand and HP operation.

**Require:** $E_{HP,SH}$, $E_{HP}^{max}$, $Q_{HP}^{max}$, $E_{app}$, $E_{PV}$, $Q_{TES}$, $Q_{TES}^{max}$, $T_{TES}$, $T_{DHW}$

{TES temperature update.}

$T_{TES} = -\frac{Q_{TES \to SH}}{C_p} + T_{TES}$

{Calculation of heat available from TES.}

$Q_{TES \to DHW} = \max\{C_p(T_{TES} - T_{DHW}), 0\}$

{Upper and lower HP operation boundaries.}

$Q_{HP,lower} = \max\{Q_{DHW} - Q_{TES \to DHW}, 0\}$

$Q_{HP,upper} = \min\{Q_{DHW} + (Q_{TES}^{max} - Q_{TES}), Q_{HP}^{max}\}$

{Excess PV production and PV based heat production (thanks to the HP).}

$COP_{TES} = f_{COP}(T_{TES} - T_{source})$ {COP is $\Delta T_{source}^{sink}$ dependent. Calculation is performed from an external function $f_{COP}$}

$E_{PV^+} = \max\{E_{PV} - E_{app} - E_{HP,SH}, 0\}$

$Q_{PV^+} = E_{PV^+} \cdot COP_{TES}$

{TES charging level update.}

$Q_{HP} = \min\{Q_{HP,upper}, \max\{Q_{PV^+}, Q_{HP,lower}\}\}$

$\Delta Q_{TES} = Q_{HP} - Q_{DHW} + Q_{TES}^{loss}$

$Q_{TES} = \max\{Q_{TES} + \Delta Q_{TES}, 0\}$

{HP operation control.}

$S = \frac{|Q_{TES}|}{Q_{TES}}$

$COP_{DHW} = f_{COP}(T_{DHW} - T_{source})$

$E_{HP,DHW} = \frac{Q_{DHW}}{COP_{DHW}} + (\Delta Q_{TES} - Q_{TES}^{loss})\frac{S-1}{-2COP_{DHW}} + (\Delta Q_{TES} - Q_{TES}^{loss})\frac{S+1}{2COP_{TES}}$

{HP operation control.}

$E_{HP} = E_{HP,SH} + E_{HP,DHW}$

**return** $E_{HP}$, $Q_{TES}$ ...

## Acronyms and abbreviations

**ASHP** Air Source Heat Pump. 20, 25, 26, 29, 30, 44

**BHE** Borehole Heat Exchanger. 14, 20, 25

**BSS** Battery Storage System. 17

**DHW** Domestic Hot Water. 29

**EH** Electric Heater. 23, 25, 29, 30, 45

**FSO** Federal Statistical Office. 19

**GIS** Geographic Information System. 19, 20

**GSHP** Ground Source Heat Pump. 14, 15, 17, 25, 26, 29, 30, 44

**HDD** Heating Degree Days. 19, 25

**HP** Heat Pump. 13–15, 17, 18, 21, 23–26, 30, 51

**HRES** Hybrid Renewable Energy System. 13, 14, 17, 18, 23, 36, 42, 44, 51

**IEA** International Energy Agency. 13, 15

**JASM** Joint Activity Scenarios and Modelling. 19

**MMH** Monthly Mean Hourly. 19, 20, 24, 51

**RegBD** Swiss National Building and Dwelling Registry. 19

**RES** Renewable Energy Source. 13–19, 51

**RMF** Residential Multi Family. 21, 29, 36, 38, 42

**RPV** Rooftop-mounted Photovoltaic. 18, 20, 21, 23, 26, 27, 29, 30, 36, 38, 42, 44, 45, 51

**RSF** Residential Single Family. 21, 24, 29, 42, 44

**SER** Service. 21, 29, 30, 44

**SH** Space Heating. 29

**SPV** Solar Photovoltaic. 13–18, 20, 29, 30, 36, 51

**STEM** Swiss TIMES Energy system Model. 19, 20, 24

**TES** Thermal Energy Storage. 17, 23, 26, 27, 29, 30, 36, 38, 40, 42, 44, 51

# Nomenclature

**Subscripts and superscripts**

| | |
|---|---|
| $d$ | Number of hours in a day. |
| $DHW$ | Domestic hot water. |
| $geo$ | Geothermal. |
| $i$ | Month. |
| $k$ | Seasonal period within winter, intermediate, or summer. |
| $L$ | Load (electrical). |
| $PV$ | Photovoltaic. |
| $rad$ | Radiator. |
| $ref$ | Reference case. |
| $seas$ | Seasonal. |
| $SH$ | Space heating. |
| $TES$ | Thermal energy storage. |
| $we$ | Weekend. |
| $wk$ | Weekday. |
| $y$ | Number of hours in a year in MMH format. |

**Symbols**

| | |
|---|---|
| $\eta$ | Energy efficiency. |
| $\Phi$ | Heat design load. |
| $A$ | Surface area. |
| $C_p$ | Isobaric thermal capacity. |
| $c_p$ | Specific isobaric thermal capacity. |
| $COP$ | Coefficient of performance. |
| $E$ | Electrical energy. |
| $EPF$ | Grid-based electricity use performance factor. |
| $m$ | Mass of transfer fluid. |
| $n$ | Number of days. |
| $PEF$ | Primary energy conversion factor. |
| $Q$ | End-use thermal energy. |
| $SCR$ | Self-consumption ratio. |
| $SSR$ | Self-sufficiency ratio. |
| $T$ | Temperature. |
| $t$ | Time. |
| $U$ | Thermal transmittance. |
| $V$ | Volume. |

# References


[1] James C. Williams. "History of Energy". PhD thesis. The Franklin Institute, 2006 (cit. on p. 13).

[2] *Energy Efficiency 2019*. https://www.iea.org/reports/energy-efficiency-2019. IEA. Nov. 2019 (cit. on p. 13).

[3] *The Critical Role of Buildings*. https://www.iea.org/reports/the-critical-role-of-buildings. IEA. Apr. 2019 (cit. on p. 13).

[4] Thibaut Abergel and Chiara Delmastro. *Tracking Buildings 2020*. https://www.iea.org/reports/tracking-buildings-2020. IEA. June 2020 (cit. on p. 14).

[5] Thibaut Abergel and Chiara Delmastro. *Building Envelopes 2020*. https://www.iea.org/reports/building-envelopes. IEA. June 2020 (cit. on p. 14).

[6] *Heating*. https://www.iea.org/reports/heating. IEA. June 2020 (cit. on p. 14).

[7] *Renewables*. https://www.iea.org/reports/renewables-2019. IEA. Oct. 2019 (cit. on pp. 14, 15).

[8] John W. Lund and Aniko N. Toth, eds. *Direct Utilization of Geothermal Energy 2020 Worldwide Review*. https://www.geothermal-energy.org/pdf/IGAstandard/WGC/2020/01018.pdf. Geo-Heat Center, Oregon Institute of Technology, USA, Ana-Geo Ltd., Hungar. Proceedings World Geothermal Congress 2020, Apr. 2020 (cit. on p. 14).

[9] OFS. *Domaine énergétique - Système de chauffage et agents énergétiques*. https://www.bfs.admin.ch/bfs/fr/home/statistiques/construction-logement/batiments/domaine-energetique.html. 2017 (cit. on p. 14).

[10] Official Journal of the European Union. *Directives on the promotion of the use of energy from renewable sources*. Tech. rep. Annex VII. European Parliament and the Council of the European Union, Dec. 2018 (cit. on p. 15).

[11] *Future of solar photovoltaïc : deployment, investment, technology, grid integration and socio-economic aspects*. https://www.irena.org/-/media/Files/IRENA/Agency/Publication/2019/Nov/IRENA_Future_of_Solar_PV_2019.pdf. IRENA. Nov. 2019 (cit. on p. 15).

[12] Jan Figgener et al. "The development of stationary battery storage systems in Germany – A market review". In: *Journal of Energy Storage* 29 (Aug. 2019). doi: 10.1016/j.est.2019.101153 (cit. on p. 16).

[13] *Energy Strategy 2050*. https://www.bfe.admin.ch/bfe/fr/home/politique/strategie-energetique-2050.html. OFEN. Nov. 2020 (cit. on p. 16).

[14] K. Shivarama and Krishna, K. Sathish Kumar. "A review on hybrid renewable energy systems". In: *Renewable and Sustainable Energy Reviews* 52 (Dec. 2015), pp. 907–916. doi: 10.1016/j.rser.2015.07.187 (cit. on p. 17).

[15] Somil Miglania, Kristina Orehouniga, and Jan Carmelieta. "Integrating a thermal model of ground source heat pumps and solar regeneration within building energy system optimization". In: *Applied Energy* 218 (Mar. 2018). doi: 10.1016/j.apenergy.2018.02.173 (cit. on p. 17).

[16] Richard Thygesen and Björn Karlsson. "Simulation and analysis of a solar assisted heat pump system with two different storage types for high levels of PV electricity self- consumption". In: *Solar Energy* 103 (Feb. 2014). doi: 10.1016/j.solener.2014.02.013 (cit. on p. 17).

[17] Daniele Testi et al. "Stochastic optimal integration of decentralized heat pumps in a smart thermal and electric micro-grid". In: *Solar Energy* 103 (Feb. 2014). doi: 10.1016/j.enconman.2020.112734 (cit. on p. 17).

[18] Alexander Thür, Toni Calabrese, and Wolfgang Streicher. "Smart grid and PV driven ground heat pump as thermal battery in small buildings for optimized electricity consumption". In: *Energy Conversion and Management* 210 (Mar. 2020). doi: 10.1016/j.solener.2018.08.087 (cit. on p. 17).

[19] Karni Siraganyan et al. "Eco-Sim: A Parametric Tool to Evaluate the Environmental and Economic Feasibility of Decentralized Energy Systems". In: *Enegies* 12 (Feb. 2019). doi: 10.3390/en12050776 (cit. on p. 17).

[20] Louis F. Cabeza et al. "CO2 mitigation accounting for Thermal Energy Storage (TES) case studies". In: *Applied Energy* 155 (Oct. 2015), pp. 365–377. doi: 10.1016/j.apenergy.2015.05.121 (cit. on p. 17).

[21] A.T.D.Perera et al. "Electrical hubs: An effective way to integrate non-dispatchable renewable energy sources with minimum impact to the grid". In: *Applied Energy* 190 (Jan. 2017). doi: 10.1016/j.apenergy.2016.12.127 (cit. on p. 17).

[22] Yu Fu et al. "A multi-objective optimization of PV/ST-GSHP system based on office buildings". In: *Energy Procedia* 152 (Jan. 2018), pp. 71–76. doi: 10.1016/j.apenergy.2016.12.127 (cit. on p. 17).

[23] John Clauss and Laurent Georges. "Model complexity of heat pump systems to investigate the building energy flexibility and guidelines for model implementation". In: *Applied Energy* 255 (Sept. 2019). doi: 10.1016/j.apenergy.2019.113847 (cit. on p. 17).

[24] Alina Walch et al. "Big data mining for the estimation of hourly rooftop photovoltaic potential and its uncertainty". In: *Applied Energy* (Aug. 2019). doi: 10.1016/j.apenergy.2019.114404 (cit. on pp. 19, 20).

[25] Sandra Sandra Settler. *Beilage "Solarkataster Schweiz: Abschätzung des Wärme- und Brauchwarmwasserbedarfs"*. Tech. rep. Annex VII. Confédération suisse, Eidgenössisches Departement für Umwelt, Verkehr, Energie und Kommunikation UVEK, Feb. 2016 (cit. on p. 19).

[26] JASM - Swiss Competence Centers for Energy Research. G. Guidati et al. *End-use energy demand - SES*. https://data.sccer-jasm.ch. Aug. 2020 (cit. on p. 19).

[27] Rammachandran Kannan and Hal Turton. *Switzerland Energy Transition Scenarios – Development and Application of the Swiss TIMES Energy System Model (STEM)*. Paul Scherrer Institut, Switzerland, Dec. 2014. url: https://www.psi.ch/sites/default/files/import/eem/PublicationsTabelle/2014-STEM-PSI-Bericht-14-06.pdf (cit. on p. 19).

[28] Ian Knight and Hajo Ribberrink. *European and Canadian non-HVAC electric and DHW load profiles for use in simulating the performance fo residential cogeneration systems*. Welsh School of Architecture, UK, Natural Resources Canada, May 2007. url: http://www.ecbcs.org/Data/publications/EBC_Annex_42_Domestic_Energy_Profiles.pdf (cit. on p. 19).

[29] M. Stokes, M. Rylatt, and K. Lomes. "A simple model of domestic lighting demand, Energy and Buildings". In: *Energy and Buildings* 36 (July 2003), pp. 103–11. doi: 10.1016/j.enbuild.2003.10.007 (cit. on p. 19).

[30] Alina Walch et al. "Quantifying the technical geothermal potential from shallow borehole heat exchangers at regional scale". Mar. 2020 (cit. on p. 20).

[31] Comission SIA. *Sondes géothermiques*. Tech. rep. SIA 384/6. Société suisse des Ingénieurs et des Architectes, Jan. 2010 (cit. on p. 20).

[32] Office fédéral: MétéoSuisse. *Station météorologique de Genève Cointrin, temperature hourly mean* (cit. on p. 20).

[33] *The Topographic Landscape Model TLM*. https://www.swisstopo.admin.ch/en/knowledge-facts/topographic-landscape-model.html. Federal Office of Topography swisstopo. 2021 (cit. on p. 21).

[34] Comission SIA. *Systèmes de chauffage dans les bâtiments – Puissance requise*. Tech. rep. SIA 384/2. Société suisse des Ingénieurs et des Architectes, June 2020 (cit. on p. 24).

[35] M. Jangsten et al. "Survey of radiator temperatures in buildings supplied by district heating". In: *Energy, The International Journal* 137 (Oct. 2016), pp. 292–301. DOI: 10.1016/j.energy.2017.07.017 (cit. on p. 24).

[36] Oliver Ruhnau, Lion Hirth, and Aaron Praktiknjo. "Time series of heat demand and heat pump efficiency for energy system modeling". In: *Scientific Data* 6 (Oct. 2019). DOI: 10.1038/s41597-019-0199-y (cit. on p. 25).

[37] Viessman France SAS. *Viessman VITOCAL - Notice pour l'étude*. Tech. rep. June 2017 (cit. on p. 26).

[38] Comission SIA. *Besoins de chaleur pour le chauffage*. Tech. rep. SIA 380/1. Société suisse des Ingénieurs et des Architectes, Dec. 2016 (cit. on p. 26).